LITHOSPHERIC DEFORMATION AND MANTLE DYNAMICS BENEATH THE EASTERN NORTH AMERICAN MARGIN FROM FREQUENCY-DEPENDENT SHEAR WAVE SPLITTING ANALYSES

by

Rajani Shrestha

A thesis submitted to the Faculty of the University of Delaware in partial fulfillment of the requirements for the degree of Master of Science in Geology

Summer 2023

LITHOSPHERIC DEFORMATION AND MANTLE DYNAMICS

BENEATH THE EASTERN NORTH AMERICAN MARGIN

FROM

FREQUENCY-DEPENDENT SHEAR WAVE SPLITTING ANALYSES

by

Rajani Shrestha

Approved: ____
Colton Lynner, Ph.D.
Professor in charge of thesis on behalf of the Advisory Committee

Approved: ____
John A. Madsen, Ph.D.
Chair of the Department of Earth Sciences

Approved: ____
Fabrice Veron, Ph.D.
Dean of the College of Earth, Ocean and Environment

Approved: ____
Louis F. Rossi, Ph.D.
Vice Provost for Graduate and Professional Education and
Dean of the Graduate College

ACKNOWLEDGMENTS

I would like to acknowledge my advisor, Dr. Colton Lynner, for his constant guidance throughout this project. Dr. Lynner's continuous support has made working on this project very rewarding and enjoyable. I am very thankful to my committee members: Dr. Jessica Warren and Dr. Maureen Long for their insights and constructive feedbacks. Thank you, Dr. Warren and Dr. Long, for being so excited to hear about my results every time. I am grateful to Dr. Andrew Birkey and Lazaro Oliva for helpful discussions. I am forever indebted to my parents, family and friends for their unwavering love, support, and belief in me and to my grandmother for being a source of constant inspiration.

This work would not have been possible without the seismic data accessed through Incorporated Research Institutions for Seismology (now EarthScope Consortium). I am sincerely thankful to the American Geophysical Union (AGU) and to the Graduate College at the University of Delaware (UD) for awarding travel grants to present this work at conferences and hence gain helpful comments.

Thanks are due to Kuan-Yu, my EmPOWER mentor, and to Karen Carlson, my CEOE Dean's Advisory Council mentor, for helping me navigate graduate school. I would like to acknowledge the entire graduate student community in the Department of Earth Sciences for offering me support whenever I needed it. I would also like to recognize all my friends, especially Tulaja, Mindy, Thabu, Kuan-Yu, Sunita, Isuri, Christy, and Prerana for making UD feel like home.

TABLE OF CONTENTS

LIST OF FIGURES

ABSTRACT

Constraints on the relative contributions of lithospheric and asthenospheric seismic anisotropy along the eastern passive margin of North America are necessary to further our understanding of past tectonics and current mantle dynamics. Previous studies have invoked several different interpretations of lithospheric and asthenospheric deformation along the margin, including vertical mantle flow, layered anisotropy, or collision-related lithospheric fabrics. The use of frequency-dependent shear wave splitting can help us distinguish between these potential interpretations. Our dataset encompasses the Appalachian Mountains in the west to the Atlantic coast in the east allowing us to investigate lateral changes in anisotropic properties. We measure shear wave splitting of teleseismic core-refracted waves recorded at seismic stations in three different frequency ranges: low (10 – 50 s), mid (5 – 10 s), and high (1 – 5 s). We observe clear frequency dependence in our results with primarily null results in the low frequency and abundant splitting in the mid and the high frequencies. In the mid and high frequencies, splitting does not correlate with plate motion. Our results instead suggest that vertically-varying anisotropy is present along the eastern US with vertical flow in the mantle beneath most of the coastal plain. Systematic backazimuthal dependence of splitting parameters further suggests layered anisotropy. We find that the anisotropic structure changes laterally with a dominantly lithospheric contribution beneath the Appalachians and a primary mantle dynamics control along the coast.

Chapter 1

INTRODUCTION

As a mature passive margin, the east coast of the US provides an ideal location (Figure 1.1) to study the deformation related to past collisional and rifting events that have shaped its present form (e.g., Aragon et al., 2017; Barruol et al., 1997b; Chen et al., 2018; Long et al., 2016). The eastern margin has undergone at least two complete Wilson cycles with the formation and subsequent breakup of the supercontinents Rodinia and Pangaea (Thomas, 2006). Deformation related to these past tectonic events reside in the lithosphere beneath the region (Barruol et al., 1997b; Brunsvik et al., 2021; Long et al., 2016). This provides an excellent opportunity to understand the deformation related to Appalachian orogenesis and whether it has been overprinted by the Mesozoic rifting of Pangaea. Further, despite being a passive margin, the mantle flow beneath this area cannot be explained by simple plate motion-driven asthenospheric shearing (Fouch et al., 2000; Yang et al., 2017). The margin is, therefore, also important in understanding how the transition from thick continental lithosphere to thin oceanic lithosphere affects the mantle flow field (Fouch et al., 2000; King & Anderson, 1998).

Both past deformation in the lithosphere and modern deformation due to asthenospheric flow can produce seismic anisotropy. Anisotropic fast directions reflect the kinematics and dynamics of deformation (Long & Silver, 2009). The distinction between anisotropic signals from lithospheric and asthenospheric sources is valuable for a clearer understanding of both past tectonics and current mantle dynamics (Long et al., 2016). This has been a fundamental question at the eastern North American Margin (ENAM) (e.g., Long et al., 2016; Wagner et al., 2012).

One of the most common methods to quantify seismic anisotropy is shear wave splitting. Splitting measurements provide two parameters: fast direction and delay time. Together, they account for the geometry and the magnitude of anisotropy that an unsplit shear wave may have traversed through to result in the observed split form (Long & Silver, 2009; Silver & Chan, 1991). The fast direction (ϕ), representing the fast axis of anisotropy, provides information on the strain orientation. The delay time (dt) between the fast and the slow waves presents a trade-off between the strength of anisotropy and the scale of anisotropic feature (Silver & Chan, 1991). Despite providing direct observations of anisotropy, shear wave splitting is a path integrated measurement and therefore does not easily constrain the depth of anisotropy (Long & Silver, 2009; M. K. Savage, 1999; Silver & Chan, 1991).

The use of multiple frequency bands in measuring shear wave splitting parameters can provide better constraints on the provenance of anisotropy and nature of anisotropic structure compared to measuring them in only one frequency range (e.g., Eakin & Long, 2013; Huang et al., 2011; Long, 2010; Marson-Pidgeon & Savage, 1997; Wirth & Long, 2010). The finite-frequency sensitivity kernels of the shear waves vary with frequency (Favier & Chevrot, 2003). Lower frequency waves sample a larger volume of medium compared to higher frequency waves (Favier & Chevrot, 2003). Therefore, low frequency waves are more sensitive to larger scale anisotropic structures (Wirth & Long, 2010). If anisotropy resides in a relatively thin layer, the lower frequency waves will be less sensitive to it because of their longer wavelengths and display no or very weak splitting.

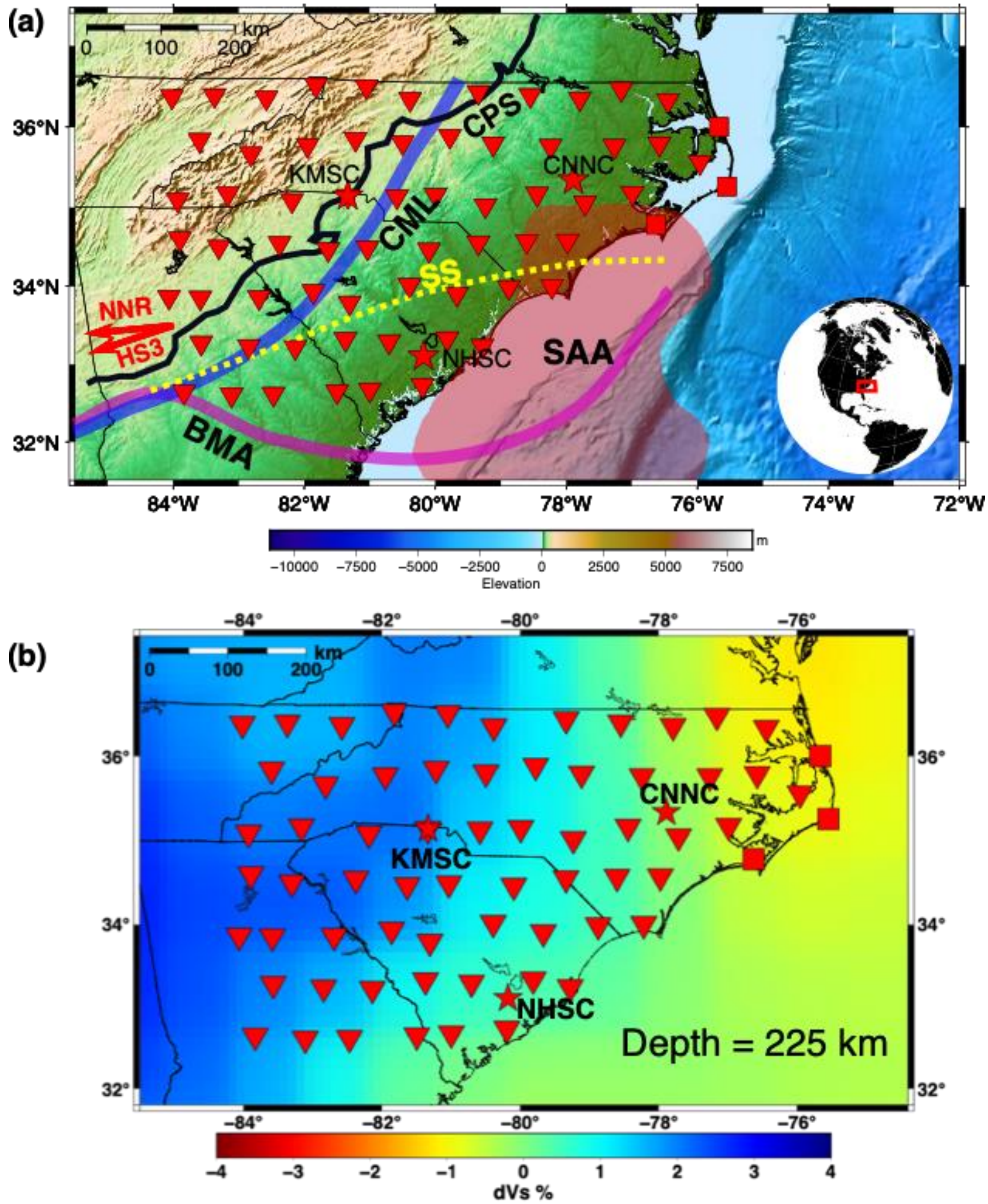

Figure 1.1 Map of the study area showing seismic stations over (a) topography and (b) shear velocity perturbations at depth 225 km (Porritt et al., 2021). Inverted triangles represent TA stations (IRIS Transportable Array, 2003), stars represent stations with ≥ 10 years of data (labeled), and squares represent ENAM-Community Seismic Experiment (CSE)

stations (Lynner et al., 2019). Arrows at the bottom left in (a) show plate motion of North America in the hotspot (HS3-NUVEL1A: Gripp & Gordon, 2002) and no net-rotation (NNR-MORVEL56: Argus et al., 2011) reference frame. In (a), thin black line represents the approximate position of Central Piedmont Suture (CPS) (Hatcher, 2007), solid blue line: Carolinia Magnetic Lineament (CML) (Hatcher, 2010), solid magenta line: Brunswick Magnetic Anomaly (BMA) (Parker, 2014), dashed yellow line: Suwanee Suture (SS) (Higgins & Zietz, 1983). The faint red area shows the approximate location of the low-velocity Southern Atlantic Anomaly (SAA) (B. Savage et al., 2017). Tomography model in (b) shows change from faster velocities beneath the Appalachian Mountains where lithosphere is thicker to slower velocities in the coastal plain with thinner lithosphere.

We measure shear wave splitting parameters at stations across the Appalachian Mountains to the Atlantic Coastal Plain from Georgia to North Carolina in the eastern US (Figure 1.1) in three different frequency ranges: low (0.02 – 0.1 Hz), mid (0.1 -0.2 Hz) and high (0.2 – 1 Hz). We include data from EarthScope Transportable Array (TA) stations (IRIS Transportable Array, 2003) as well as permanent US network stations (Albuquerque Seismological Laboratory (ASL)/USGS, 1990) and the coastal stations from ENAM-Community Seismic Experiment (CSE) (Lynner et al., 2019) to analyze the frequency-dependent splitting across the margin. Frequency dependence of the splitting parameters indicate complex anisotropic structure with vertically- or laterally-varying anisotropy (Rümpker & Silver, 1998; Saltzer et al., 2000; Wirth & Long, 2010).

Chapter 2

BACKGROUND

2.1 Tectonic Setting

The passive margin to the east of the US was formed due to the rifting of Pangaea ~200 million years ago (Schlische, 2003; Thomas, 2006; Withjack et al., 2012). The earlier collisional events during the assembly of Pangaea, culminating in the Alleghenian orogeny, formed the Appalachian Mountains (Hatcher, 2007, 2010). Subsequent rifting opened the Atlantic Ocean forming the passive margin as we see today (Thomas, 2006). The rifting is associated with the Central Atlantic Magmatic Province (CAMP) volcanism at the Triassic-Jurassic transition (Marzoli et al., 2018 and references therein), which resulted in abundant diking in the southeastern US (Ragland et al., 1983). In contrast to the northern part of the passive margin outside of our study region, the southeastern US exhibits the nature of a volcanic margin with the presence of seaward-dipping reflectors (SDRs) in the crust (Schlische, 2003; Withjack & Schlische, 2005). SDRs along the eastern margin are generally associated with the offshore East Coast Magnetic Anomaly (ECMA) formed during rift-drift transition (Davis et al., 2018). The landward extension of SDRs is also present in several locations in southeastern US (e.g. Crossroads Basalt in Benson, 2003; Davis et al., 2018). The margin has been relatively stable with no major deformational events since breakup (Schlische, 2003; Withjack & Schlische, 2005) so any rift-related deformational features should remain preserved within the lithosphere (Brunsvik et al., 2021).

The eastern North American margin (ENAM) contains several tectonic features and accreted terranes owing to its complex history (Thomas, 2006; Hibbard et al., 2007; Hatcher, 2010). In our study area (Figure 1.1), the southern Appalachian Mountains are the major tectonic unit and consist of: (a) the Blue Ridge Mountains, (b) the Inner Piedmont Terrane, and (c) the Carolina Superterrane (or Carolinia) from west to east (Hatcher, 2010; Hibbard et al., 2007). In contrast to the high elevations of the Appalachians, the Atlantic coastal plain to the east is a low-lying feature that extends offshore. The coastal plain has a thick, transitional crust that separates the thicker continental crust from the thinner oceanic crust (C. Li & Gao, 2021; Lynner & Porritt, 2017). The crust is thickest beneath the Blue Ridge Mountains reaching up to 55 km (Parker et al., 2013). Crustal thickness varies between 34 – 37 km along the coast and decreases to 30 km near the continent-ocean transition (W. Guo et al., 2019). Similarly from west to east, the lithospheric thickness decreases from 220-250 km in the North American craton to ~100-200 km beneath the Appalachians (van der Lee, 2002; Yuan et al., 2011). Although seismic lithosphere-asthenosphere boundary beneath the coastal plain is interpreted to be <150 km, high resistivity values observed beneath the Piedmont and the Atlantic Coastal Plain in magnetotelluric studies has been argued to represent a thicker (~200 km) lithosphere beneath the margin (Murphy & Egbert, 2019).

Magnetic anomalies associated with different stages of margin evolution are present along the east coast, both onshore and offshore (e.g., Boote et al., 2018; Duff & Kellogg, 2019; Higgins & Zietz, 1983; Parker, 2014; Taylor et al., 1968; Wagner et al., 2012). The Brunswick Magnetic Anomaly (BMA) is a prominent negative magnetic anomaly which runs nearly E-W across southern Georgia before turning almost N-S offshore (Higgins & Zietz, 1983). The BMA is interpreted to either represent an Alleghenian suture between the Charleston and the Suwannee terranes (Parker, 2014) or be associated with a mafic intrusive body formed during Mesozoic rifting (Duff & Kellogg, 2019). The Higgins-Zietz boundary further north is regarded as the Suwannee Suture (SS) representing the boundary delineating pre-Alleghenian Laurentia from the Charleston and the Suwanee terranes (Marzen et al., 2019). The Carolinia Magnetic Lineament (CML) is a NE-trending feature that goes across central Georgia, South Carolina and North Carolina (Wagner et al., 2012). The CML is related to the Central-Piedmont Suture (CPS) separating Carolina superterrane from Laurentian terranes of the Inner Piedmont (Hatcher, 2010). Lineament-parallel anisotropic signals previously observed along the margin have been interpreted to be due to strong, localized lithospheric anisotropy related to the tectonic history of the region (Long et al., 2016; Wagner et al., 2012).

2.2 Seismic Anisotropy

Observations of seismic anisotropy are widely used to study deformation inside the earth (Fouch & Rondenay, 2006; Long & Becker, 2010; Long & Silver, 2009; M. K. Savage, 1999). Coherent deformation in the earth's upper mantle can produce bulk seismic anisotropy (i.e., the directional dependence of seismic wave velocity). Seismic anisotropy is typically due to lattice-preferred orientation (LPO)/crystal-preferred orientation (CPO) of minerals in the mantle (Karato et al., 2008), or due to shape-preferred orientation (SPO) of structures such as stress-aligned cracks in the crust (Crampin and Lovell, 1991; Crampin and Chastin, 2003). The average anisotropy observed for shear waves is between 2% and 4% in the upper mantle (Dziewonski and Anderson, 1981; Savage, 1999). Although anisotropy values range from 1.5 to 4% in the upper crust (Crampin, 1994; M. K. Savage, 1999), there is negligible contribution to shear wave splitting measurements from crustal anisotropy (i.e., around 0.1 – 0.3 s) when compared to the total splitting delay times, which are normally around a second (Crampin, 1994; Fouch & Rondenay, 2006; M. K. Savage, 1999; Silver, 1996).

In the upper mantle, asthenospheric flow produces lattice-preferred orientation (LPO) of olivine, the primary constituent of the mantle by volume. Olivine is inherently anisotropic and has faster seismic velocities along its a-axis [100] (Karato et al., 2008). The maximum shear anisotropy for a single olivine crystal can reach up to 18% (Mainprice et al., 2000). Plastic deformation of olivine under dislocation creep aligns its fast direction in a preferred orientation to produce different kinds of anisotropic olivine fabrics (Karato et al., 2008). Olivine fabrics define the relation of the fast axis of anisotropic feature to the strain field. Five major types of fabric have been identified from mineral physics studies: A-, B-, C-, D- and E-type (Jung & Karato, 2001; Karato et al., 2008; Katayama et al., 2004). For horizontal flow, A-, C-, D- and E-type fabrics align fast axes along the direction of mantle flow while B-type fabric aligns fast direction perpendicular to flow (Karato et al., 2008; Lynner et al., 2017).

The type of olivine fabric formed depends on stress, temperature, and water content in the mantle (Karato et al., 2008). A-, C- and E-type fabrics are all associated with high temperatures and low-moderate stress conditions with varying water content; D- type fabric requires high stress and low water content while B-type fabric is formed under conditions of high stress and high water content (Karato et al., 2008). It has been shown that B-type fabric is mostly related to mantle wedges at cold subduction zones (Kneller et al., 2005). Due to the nature of ENAM, we do not expect high-stress conditions and therefore B- and D-type fabrics are unlikely. A-, C- or E-type fabrics are the best candidates for mantle flow beneath ENAM (Long et al., 2010; Lynner & Bodmer, 2017). These three fabrics produce similar splitting patterns for the nearly vertical seismic phases used in this study where fast directions are parallel to the flow direction (Lynner et al., 2017).

The parallelism of shear wave splitting measurements with structural fabrics instead of plate motion presents an important case for frozen-in or fossil lithospheric anisotropy (Vauchez & Barruol, 1996). Orogen-parallel fast directions could result from preferred alignment of slow olivine b-axis parallel to the direction of maximum compression (Silver & Chan, 1988), simple shear due to strike-slip deformation (Vauchez & Nicolas, 1991) or rift-parallel mantle flow during pre-orogenic rifting (Nicolas, 1993). The correlation of fast axis of anisotropy with magnetic features has been interpreted to be due to vertically coherent deformation in the crust and the mantle lithosphere (e.g., Wüstefeld et al., 2010). The change in anisotropic properties over short lateral distances, and the similarity of fast directions within tectonic units versus their variation between tectonic units provide evidence for the presence of significant lithospheric anisotropy (Barruol et al., 1997a; Barruol et al., 1997b; Wüstefeld et al., 2010).

Lithospheric anisotropy along ENAM could be associated with the Appalachian mountain-building, terrane accretion during the formation of Pangea, and/or fossil CPO from the extension and rifting of Pangea (Brunsvik et al., 2021; Long et al., 2016; Russell & Gaherty, 2021; Wagner et al., 2012). If preserved, anisotropy related to the Appalachian orogenesis will have orogen-parallel fast directions (e.g., Long et al., 2010, 2016; M. K. Savage, 1999; Silver, 1996). Anisotropy associated with the Mesozoic rifting could be parallel to the extension direction (Eilon et al., 2014; Tommasi et al., 1999) or the rift axis (Vauchez et al., 2000). There could be paleo-plate motion induced anisotropy in the lithosphere (Deschamps et al., 2008; Yuan & Romanowicz, 2010) although this is more likely to occur in the oceanic setting where new lithosphere is being formed (Russell & Gaherty, 2021). Anisotropy related to various stages of the formation of Pangaea could parallel magnetic features and/or sutures (Wagner et al., 2012). Even though crustal anisotropy might be present, the most significant contribution to ~1 s splitting times previously measured in the region is due to anisotropy in the lithospheric and asthenospheric mantle (Long et al., 2016; Yang et al., 2017).

2.2.1 Shear Wave Splitting

Shear wave splitting provides one of the most direct observations of seismic anisotropy in the earth (Fouch & Rondenay, 2006; Long & Silver, 2009). When a shear wave passes through an anisotropic medium, like the mantle, it is split into two orthogonal quasi-S components (Silver, 1996). The polarizations of the quasi-S waves are dependent upon the orientation of anisotropy, and one of them travels faster than the other (Long & Silver, 2009; Silver, 1996). Moving through the medium, these components accumulate increasing delay time between each other. If a polarized shear wave traveled through an isotropic mantle, it would record a linear particle motion in the seismogram and no accrued delay time. On the other hand, split shear waves register an elliptical particle motion because of the delay time between the two quasi-S components (Silver, 1996; Silver & Chan, 1991). Shear wave splitting techniques search for the values of fast direction and delay time which can best correct the elliptical particle motion (Bowman & Ando, 1987; Silver & Chan, 1991; Wüstefeld et al., 2008).

The fast direction (ϕ) and delay time (dt) from splitting are observational parameters for the geometry and strength of anisotropy, respectively. The fast direction (ϕ) corresponds to the polarization of the faster quasi-S wave and gives the anisotropic fast axis. The delay time (dt) is the time lag between faster and slower quasi-S components and is related to both the strength of anisotropy as well as the layer thickness (Fouch & Rondenay, 2006; Long & Silver, 2009). A thicker layer having some value of shear wave anisotropy may produce similar delay times as a thinner layer having stronger anisotropy. For example, although both the upper crust and upper mantle are expected to have ~2-4% of anisotropy in general, the splitting times associated with mantle anisotropy is in the order of a second while the delay time for crustal anisotropy generally ranges from 0.1-0.3 seconds due to the crust being a much thinner layer than the upper mantle (Crampin, 1994; Fouch & Rondenay, 2006; M. K. Savage, 1999; Silver, 1996).

Upper mantle anisotropy is commonly studied by measuring the splitting of core-refracted body wave phases: SKS, SKKS, and PKS, collectively called XKS phases (e.g., Chen et al., 2018; Fouch et al., 2000; Long et al., 2010, 2016; Wagner et al., 2012; Yang et al., 2017). These phases are converted from P- to SV-waves during refraction across the core-mantle boundary, implying that any observed anisotropy must be on the receiver-side of the ray path. This conversion also sets the initial polarization of the unsplit S-wave, which corresponds to the backazimuth. Further, the near-vertical incidence in the upper mantle of these core-refracted XKS phases samples anisotropy directly beneath the recording station and provides excellent lateral resolution when stations are nearby (Long & Silver, 2009), such as with the Transportable Array.

For lower frequencies (10-25 s), the delay times due to mantle anisotropy is generally ~1s while the contribution from crustal anisotropy is ~0.1-0.3 seconds (Crampin, 1994; M. K. Savage, 1999). Studies of mantle anisotropy generally neglect the contribution of crustal anisotropy over long periods even though it is a potential contaminant (Long & Silver, 2009; M. K. Savage, 1999). For higher frequencies (1-5 s), the delay times are generally smaller (Wirth & Long, 2010) and therefore the contribution from crustal anisotropy may become more important.

When there is no apparent splitting, but a strong XKS arrival is present, it is deemed a null measurement. Although nulls do not provide any anisotropic parameters, they are useful to evaluate potential scenarios concerning anisotropy. The simplest explanation for nulls is the lack of anisotropy. Isotropy in the upper mantle is unlikely as ENAM has a complex tectonic history and the North American plate is currently moving roughly towards the southwest: ~252° in the hotspot reference frame (Gripp & Gordon, 2002) and ~270° in the no net-rotation reference frame (Argus et al., 2011) (Figure 1.1). A lack of anisotropy is not a likely explanation for null measurements along the margin (Long et al., 2010, 2016).

Another situation producing nulls is when the initial polarization of shear wave coincides with the fast or slow axes of anisotropy (Wüstefeld & Bokelmann, 2007). If the backazimuths for nulls are dominantly in a specific direction, we could interpret it as the fast/slow direction (e.g., Wirth & Long, 2010) provided that the event distribution is widespread across backazimuths. Nulls over a range of backazimuths can result if there is vertical flow in the mantle (e.g., Lynner & Bodmer, 2017; Wagner et al., 2012). Core-refracted body waves have near-vertical ray paths (Long & Silver, 2009) and these waves will experience no splitting if the fast direction is vertical. Lastly, widespread nulls can indicate the presence of multiple layers of anisotropy that destructively interfere (Long et al., 2010).

Despite providing direct observations of the magnitude and direction of anisotropy, shear wave splitting is limited by poor depth resolution due to vertically incident raypaths and to it being a path integrated measurement (Long & Silver, 2009). We rely on the comparison of splitting parameters with tectonic features, absolute plate motion, and other geological observations to interpret likely causes and sources of anisotropy (e.g., Long et al., 2016; Yang et al., 2017). In eastern North America, this is complicated due to the presence of multiple potential anisotropy sources. Additionally, expected anisotropic directions from several sources may be in alignment, such as topographic features like the Appalachians running almost parallel to the direction of absolute plate motion (e.g., Barruol et al., 1997b; Silver, 1996; Wagner et al., 2012).

2.2.2 Anisotropy beneath the ENAM: Previous Studies

Several studies have investigated the anisotropy beneath the eastern margin using shear wave splitting (Aragon et al., 2017; Barruol et al., 1997b; Fouch et al., 2000; Levin et al., 1999; Long et al., 2010, 2016; Wagner et al., 2012; White-Gaynor & Nyblade, 2017a; Yang et al., 2017), surface waves (Deschamps et al., 2008; Gaherty, 2004; Wagner et al., 2018), P-wave anisotropic tomography (Liang et al., 2022), and joint inversion of surface or teleseismic body wave phases with splitting (Brunsvik et al., 2021; Yuan et al., 2011). We will discuss the general splitting patterns observed previously and then move on to the observations from surface wave and other joint tomographic studies.

NE-SW fast orientations have been observed over most of the eastern margin (Figure 2.1) (Barruol et al., 1997b; Long et al., 2016; Yang et al., 2017). This is sub-parallel to the North American plate motion in the hotspot reference frame (Gripp & Gordon, 2002). The plate motion-parallel fast directions are also parallel to the structural trend of the Appalachian orogen (Barruol et al., 1997b; Long et al., 2016). Barruol et al. (1997b) proposed a significant lithospheric contribution based on the correlation of the splitting delay times with the lithospheric thickness and the variation in splitting parameters over short distances. Wagner et al. (2012) observed that at several stations the fast directions match the trend of magnetic anomalies and may represent the lithospheric deformational fabric. This implies that contributions from both lithosphere and asthenosphere to the splitting results are plausible (Long et al., 2016).

In the southeastern coastal plain, a dominance of nulls (Long et al., 2016; Wagner et al., 2012) as well as presence of N-S oriented splits (Yang et al., 2017) have been reported (Figure 2.1). The coastal null stations could be due to anisotropic fabric weakened by magmatic intrusion during the Mesozoic rifting (Barruol et al., 1997b). Alternately, the null measurements could be due to vertical or incoherent mantle flow or multiple layers of anisotropy that effectively cancel each other out (Long et al., 2010, 2016; Wagner et al., 2012). E-W fast directions that rotate to NE-SW have been observed in southern Alabama, Georgia and South Carolina (Long et al., 2016; Yang et al., 2017). This could indicate fossil fabric related to the accretion of Suwanee terrane (Long et al., 2016; Wagner et al., 2012) or could be due to the interaction between plate motion parallel and keel-deflected flow in the mantle (Yang et al., 2017).

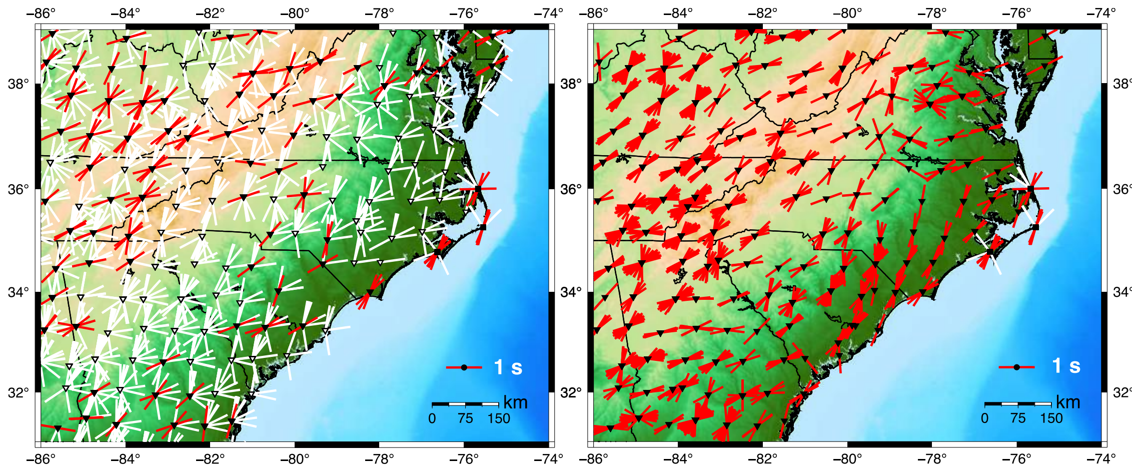

Figure 2.1 Individual splitting measurements from Long et al. (2016) (left) and Yang et al. (2017) (right) at onshore stations (triangles). Splitting at ENAM-CSE stations (squares) from Lynner and Bodmer (2017) is included in both. Red lines = fast directions of non-null splits and white lines = backazimuth of nulls. Long et al. (2016) used a bandpass filter of (0.02-0.125 Hz) and Yang et al. (2017) used (0.04-0.5 Hz). Note the discrepancy between Long et al. (2016) and Yang et al. (2017) with stations producing mostly nulls in the former and splits in the latter.

Long et al. (2016) identified several distinct anisotropic regions based on the splitting patterns. Fast polarization directions parallel the strike of the Appalachian orogen, including a bend near the Pennsylvania Salient. Predominantly null stations are present in the eastern part around North Carolina. There are fewer splits with greater than average delay times in southern Georgia and South Carolina. The fast directions following a clear bend associated with the Pennsylvania Salient support the presence of lithospheric anisotropy (Long et al., 2016; White-Gaynor & Nyblade, 2017a). In the southern part, the pattern of the fast directions resembles the pattern of Brunswick Magnetic Anomaly (BMA) even though the stations are not very close to the actual magnetic lineament (Long et al., 2016). The observations of mostly nulls might be due to the presence of complex anisotropy or vertical/incoherent flow in the mantle (Long et al., 2016).

In contrast, Yang et al. (2017) observed margin-parallel fast orientations in the coastal stations in the southeastern US when they used a slightly higher frequency range of 0.04-0.5 Hz compared to 0.02-0.125 Hz used by Long et al. (2016). In the Appalachian Mountains, Yang et al. (2017) also observed NE-SW fast directions similar to Long et al. (2016). However, to the east of the orogen, they observed ~N-S fast splitting directions in contrast to the predominantly null measurements reported in the Long et al. (2016) study. Yang et al. (2017) proposed a primarily asthenospheric contribution to anisotropy based on the disagreement between fast directions and geological trends, the presence of higher splitting times in regions with thin lithosphere, and the lack of increase in delay times near major terrane boundaries. The deviation between fast directions and absolute plate motion (APM) direction along the margin in the hotspot reference frame (Gripp & Gordon, 2002) could be explained by mantle flow deflected around the edges of the North American cratonic keel (Fouch et al., 2000; Yang et al., 2017). The N-S fast direction near the coast is interpreted to be the margin-parallel component of the edge-driven convection invoked by the contrast in lithospheric thickness across the margin (Brunsvik et al., 2021; Kaislaniemi & van Hunen, 2014; King & Anderson, 1998).

From joint inversion of surface waves and shear wave splitting data, Yuan and Romanowicz (2010) proposed two layers of anisotropy in the lithosphere and a third layer in the asthenosphere for the North American craton. The upper lithospheric layer has fast directions parallel to the geological trends and tapers out near the edge of the craton in the Atlantic Coastal Plain where the deeper lithospheric layer becomes the sole contributor to the lithospheric anisotropy. Yuan and Romanowicz (2010) observed generally N-S trending fast polarization directions in this lower layer which they interpreted to be either due to east-west compression or due to northward paleo-plate motion of the North American plate during the Mesozoic rifting of Pangaea. The asthenospheric layer has approximately APM-parallel fast directions (Yuan & Romanowicz, 2010). Three anisotropic layers related to the Appalachian orogenesis, NNW paleo-plate motion after the orogenesis and APM-parallel flow have also been observed from Rayleigh wave dispersion studies (Deschamps et al., 2008). The backazimuthal variation of splitting parameters observed further north of our study area also support the presence of multiple layers of anisotropy (Aragon et al., 2017; Levin et al., 1999).

Joint anisotropic tomography revealed layered anisotropic structure over most of the south-eastern margin (Brunsvik et al., 2021). Brunsvik et al. (2021) observed margin-perpendicular fast axes in the lithosphere and margin-parallel fast axes in the asthenosphere beneath western North Carolina/South Carolina. The margin-perpendicular lithospheric anisotropy could be related to either previous collision or rifting events (Brunsvik et al., 2021). In contrast, at the eastern North Carolina/South Carolina border, margin-parallel fast directions were observed both in the lithosphere and the asthenosphere (Brunsvik et al., 2021). This strong ~N-S splitting (Brunsvik et al., 2021; Yang et al., 2017) could be due to both lithospheric and asthenospheric fabrics aligning parallel to the margin (Brunsvik et al., 2021). Margin-parallel splitting has also been observed offshore and attributed to modified modern-day mantle flow (Brunsvik et al., 2021; Lynner & Bodmer, 2017). The prevalence of margin parallel splitting across the continent-ocean transition suggest that mantle flow is being affected by the lithospheric step as the lithosphere thins out offshore (Brunsvik et al., 2021; Lynner & Bodmer, 2017).

2.2.3 Anisotropy and Mantle Dynamics

Anisotropy driven by shear at the base of the plate from tectonic plate motion cannot explain the complex splitting patterns observed along the eastern margin (Fouch et al., 2000; Long et al., 2010, 2016; Wagner et al., 2012; Yang et al., 2017). One possibility for the deviations from plate motion could be mantle flow deflected horizontally around the thick continental keel of North America (Fouch et al., 2000). Interactions between plate-motion induced flow and keel-deflected flow could cause splitting that varies at different locations along the margin (Yang et al., 2017). This could explain why we get E-W fast directions in southern Alabama and N-S fast directions at the coastal plain to the east of the Appalachian Mountains (Yang et al., 2017). The edge-driven convection system that forms due to temperature gradients produced by contrasts in lithospheric thickness (King & Anderson, 1998) could explain the ~N-S splitting fast directions and the slow velocity anomalies present along the margin (Brunsvik et al., 2021).

The abundance of null measurements in the southeastern US could imply vertical flow in the mantle (Long et al., 2010). Based on the striking lateral variation in splitting from NE-SW aligned fast directions in the Appalachian Mountains to null stations in the coast, Long et al. (2010) proposed that a different mantle flow dynamics is required to the east of the mountains. Long et al. (2010) attributed the presence of null stations to vertical flow, either associated with downwelling due to edge-driven convection (King, 2007; King & Anderson, 1998) or with hydrous upwelling from the subducted Farallon slab (van der Lee et al., 2008). Wagner et al. (2012) obtained similar results and suggested vertical or incoherent flow beneath the margin. Vertical flow along the margin is further supported by the presence of multiple low velocity anomalies along the margin (Biryol et al., 2016; Brunsvik et al., 2021; Carrero Mustelier & Menke, 2021; Pollitz & Mooney, 2016; B. Savage, 2021; B. Savage et al., 2017). These anomalies could be due to upwellings from edge-driven convection cells (King, 2007; King & Anderson, 1998; King & Ritsema, 2000), upwelling of hydrous materials from the subducted Farallon slab (van der Lee et al., 2008), upwelling associated with lithospheric loss/delamination (Biryol et al., 2016; Mazza et al., 2014) or shear-driven upwelling (Evans et al., 2019; Long et al., 2021).

In our study region, a low shear velocity anomaly has been reported off the coast of North Carolina-South Carolina (Figure 1.1) (B. Savage et al., 2017). A reduced P-velocity anomaly is located in the coastal plain in South Carolina and northern Georgia (Biryol et al., 2016). A low velocity region around this area can also be detected at ~100 km depth in the S-wave tomographic model by van der Lee & Nolet (1997) and at~275 km in the model by Brunsvik et al. (2021). Further north of our study region, the Central Appalachian Anomaly (Schmandt & Lin, 2014) or the Harrisonburg Anomaly (Brunsvik et al., 2021) has been interpreted as mantle upwelling related to edge-driven convection (Brunsvik et al., 2021), lithospheric delamination (Biryol et al., 2016) or shear-driven upwelling (Brunsvik et al., 2021; Long et al., 2021). Similarly, the low-velocity anomaly beneath our study region has been interpreted as edge-driven convection upwelling (B. Savage et al., 2017) or upwelling due to return flow associated with lithospheric delamination further west (Biryol et al., 2016). The edge-driven convection cells are formed due to the temperature gradient arising from the contrast in lithospheric thickness (King, 2007; King & Anderson, 1998). The N-S margin-parallel anisotropy along the coast have been interpreted as a component of the 3D edge-driven convection which forms convection rolls perpendicular to the strike of the margin (Brunsvik et al., 2021; Kaislaniemi & van Hunen, 2014; Liang et al., 2022). The discrepancy in the anisotropy observations and therefore the consequent interpretation of mantle dynamics beneath the region warrants a more comprehensive investigation of anisotropy beneath the eastern passive margin.

2.3 Frequency-dependent Shear Wave Splitting

Frequency dependent splitting has been used to study complex anisotropy in regions where multiple sources is expected (Eakin & Long, 2013; Huang et al., 2011; Long, 2010; Marson-Pidgeon & Savage, 1997; Wirth & Long, 2010). Frequency-dependent splitting is based on the principle that different frequencies have different sensitivities to different scales of anisotropic features (Favier & Chevrot, 2003; Long & Silver, 2009; Wirth & Long, 2010). Lower frequency waves, owing to their longer wavelengths are less sensitive to thinner anisotropic features. It is possible that if the anisotropic layer is sufficiently thin, its effect will be smoothed out in the low frequency regime so that little effective splitting is seen (Wirth & Long, 2010). The high frequency waves, on the other hand, experience anisotropy present in thinner as well as thicker layers. The analysis of change in splitting behavior with frequency could help us evaluate potential implications for anisotropy (Figure 2.2).

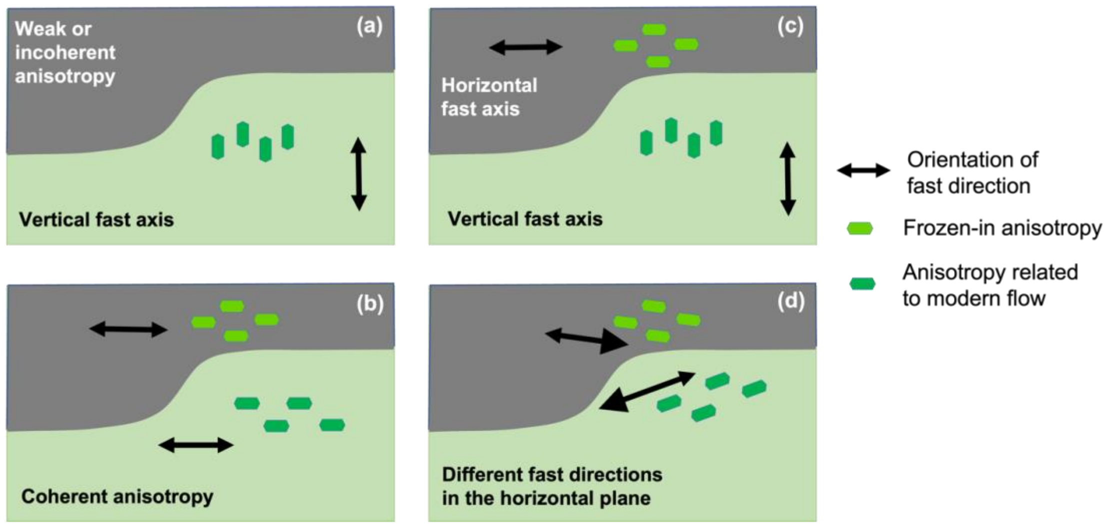

Figure 2.2 Possible anisotropic geometries with depth that could result in: (a), (b) no frequency dependence; and (c), (d) frequency dependence in splitting parameters. (a) weak anisotropy in the upper layer (presumably lithosphere) with vertical flow in the asthenosphere; (b) similar anisotropic geometry in both layers; (c) horizontal axis of anisotropy in the lithosphere and vertical flow in the asthenosphere; (d) different anisotropic properties in the lithosphere and the asthenosphere.

If splitting parameters are similar in all three frequencies, it may mean consistent anisotropic fabric in the lithosphere and asthenosphere or that anisotropy is present in only one layer that all the three frequencies are sampling. Dominantly null results in all frequencies could mean isotropy or strengthen the hypotheses of vertical mantle flow. Nulls in the lower frequency and splits in higher frequencies could indicate vertical mantle flow and shallower anisotropic layer. If splitting directions and delay times are different across frequencies, multi-layered anisotropy with different anisotropic geometries could be present. The change of splitting parameters with frequency, i.e., frequency dependence, is evidence for vertically varying anisotropy (Eakin & Long, 2013; Huang et al., 2011; Long, 2010; Marson-Pidgeon &

Savage, 1997; Wirth & Long, 2010). Although frequency-dependence can also mean the presence of lateral heterogeneities (Marson-Pidgeon & Savage, 2004), it would require that the splitting parameters vary significantly among adjacent stations (Wirth & Long, 2010).

Chapter 3

DATA AND METHODS

We measure shear wave splitting for core-refracted phases-PKS, SKS and SKKS (or XKS phases) across three frequency bands: low (0.02-0.1 Hz), mid (0.1-0.2 Hz) and high (0.1-1 Hz). The analyzed seismic stations are located in the southeastern US from Georgia to North Carolina roughly between the latitudes of 32°N and 37°N and the longitudes of 75°W and 85°W (Figure 1.1). We use broadband seismic data recorded by 62 temporary TA stations (IRIS Transportable Array, 2003), 3 coastal ENAM-CSE stations (Lynner et al., 2019), and 3 permanent stations (Albuquerque Seismological Laboratory (ASL)/USGS, 1990). The TA stations were in operation from 2012 to 2015 and each station has around 2 years' worth of data (Figure 3.1). Long running US stations have between 10 to 20 years of data with CNNC running from 2006 to 2018, KMSC from 2008 to 2018 and NHSC from 2001 until present. The ENAM-CSE stations have ~1 year of data.

The interstation spacing of ~70 km for the TA provides good lateral resolution for studying lithosphere- and asthenosphere-scale features. The core-refracted phases-PKS, SKS and SKKS (collectively called XKS) record receiver-side splitting, have near-vertical incidence, and known initial polarization (Long & Silver, 2009). The study area spans from the Appalachians to the coast and hence incorporates the lateral variations in anisotropy observed in previous studies (e.g., Long et al., 2016; Yang et al., 2017). For each station, earthquakes within the epicentral distance of 90° to 145° with a magnitude greater than or equal to 5.8 are selected to ensure that waveforms with enough energy in XKS phases are obtained (Figure 3.1). The station orientations recorded at IRIS Data Management Center (DMC) are used to correct for misorientations.

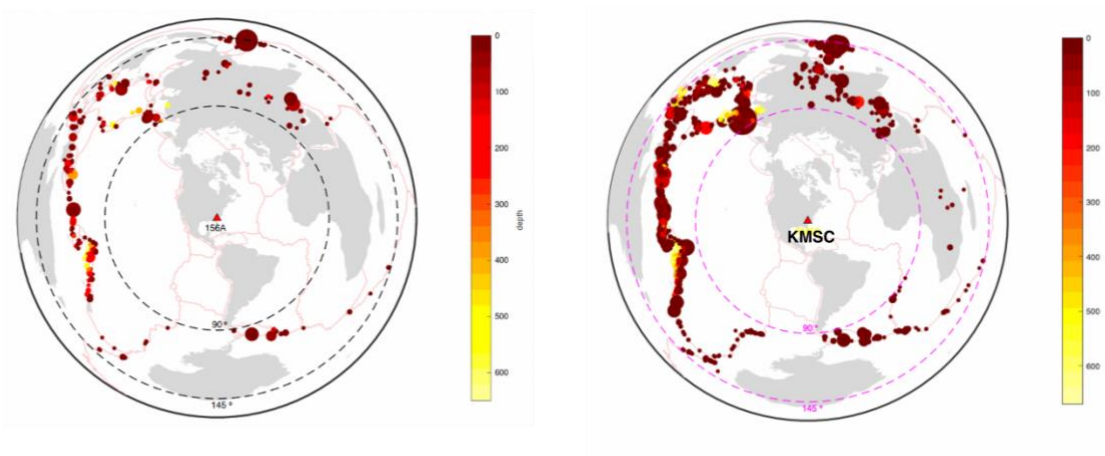

Figure 3.1 Example of event distribution map for stations 156A and KMSC shows the difference in amount of data as well as backazimuthal coverage between temporary TA (e.g., 156A) and long-run stations (e.g., KMSC). The size of plotted circle corresponds to the magnitude of earthquake. The dashed circular outlines mark epicentral distances of 90° and 145° from the station.

3.1 Shear Wave Splitting

We use the SplitLab software package (Wüstefeld et al., 2008) to obtain the splitting parameters: fast direction (ϕ) and delay time (dt). Both transverse component minimization, hereafter called SC, (Silver & Chan, 1991) and rotation-correlation, hereafter called RC, (Bowman & Ando, 1987) methods are used. The use of multiple methods to get splitting parameters increases the reliability of measurements (Long & Silver, 2009). The results from the SC method are used for further analyses and results from RC are used to ensure the quality of measurements. Only those splits that have agreements between the two methods, within 15° in fast directions and 0.4 seconds in delay time, are taken for further analyses.

While traveling through the anisotropic earth, the split quasi-S waves accumulate a delay time corresponding to the strength of anisotropy and the length of path in the anisotropic feature. When this delay is much less than the dominant wave period, the shear wave exhibits elliptical particle motion (M. K. Savage, 1999; Silver & Chan, 1991). To correct for the splitting, the transverse component minimization method finds the pair of fast direction (ϕ) and delay time (dt) that minimized the amount of energy on the transverse component (Silver & Chan, 1991). The rotation-correlation method uses a grid-search approach to find a pair of ϕ and dt for which the cross-correlation coefficient between the corrected horizontal components is maximized (Bowman & Ando, 1987; Long & Silver, 2009). The SC method is more reliable for noisy datasets but requires the initial polarization to be known (Long & Silver, 2009).

To maintain the quality and reliability of splitting measurements, we follow a series of quality control steps. We bandpass filter each waveform in individual frequency bands and visually inspect the filtered seismograms to ensure they have high signal-to-noise ratio and clear arrivals in the XKS phases. We then select an appropriate time window around the arrival to get the splitting parameters and characterize the splits as good, fair, or poor based on the signal-to-noise ratio and errors in splitting parameters. Splits within ±30° of maximum error in fast direction and up to ±1 s of error in delay time are classified as fair splits, similar to Long et al. (2010). Splits that exhibit a very high signal-to-noise ratio, have an elliptical particle motion and linear corrected motion, and have very well-constrained errors (±20° in ϕ

and ±0.5 s in dt) are classified as good splits (Figure 3.2). The good and fair splits are taken collectively for further analysis.

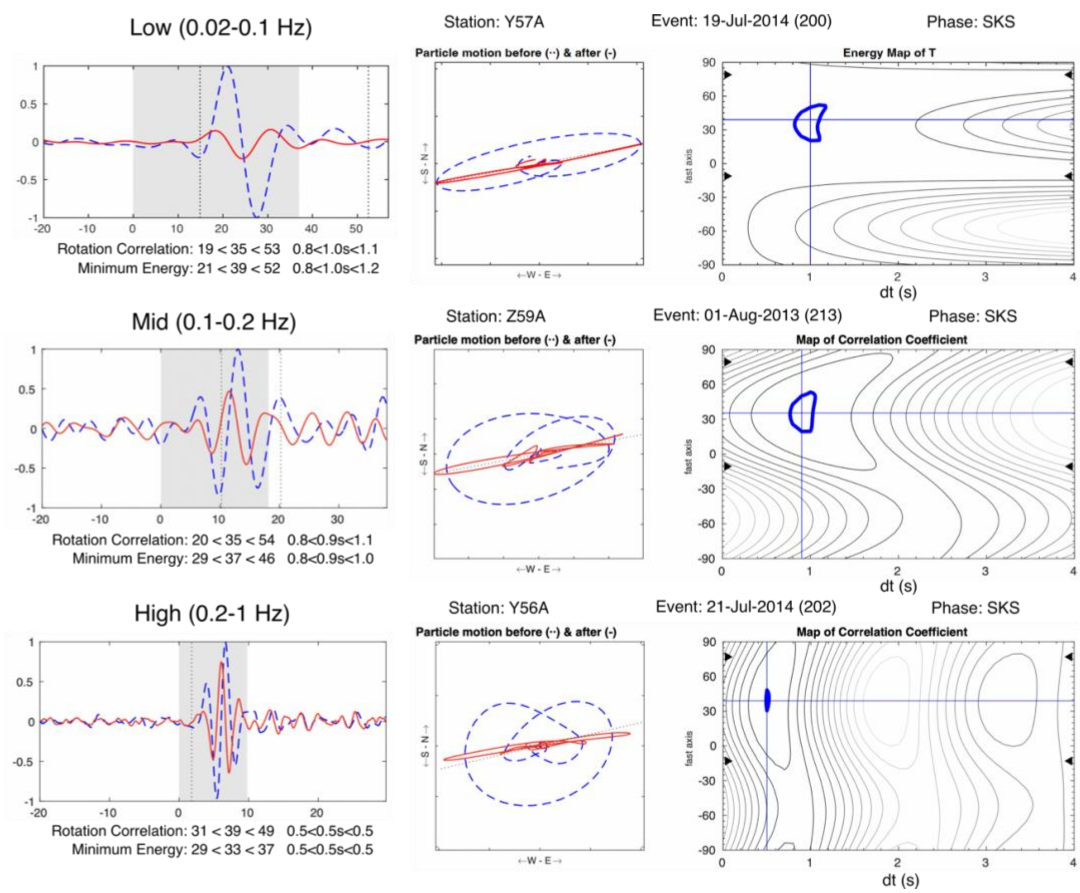

Figure 3.2 Examples of good splits in low, mid, and high frequencies (from top to bottom). The left panel shows SKS waveform with radial (dashed blue line) and transverse (solid red line) components; greyed-out area is the time window; ϕ and dt with 2σ errors are provided below the seismograms. The mid panels have initial (dashed blue) and corrected (solid red) particle motions for minimum energy method (Silver & Chan, 1991). The panels to the left show error surfaces with 95% confidence region in blue.

We record null measurements based on the linearity of the initial particle motion (Long et al., 2010, 2016; Wüstefeld & Bokelmann, 2007). We categorize nulls as good, fair, or poor. A good null has an XKS phase with a good signal-to-noise ratio, a clear arrival in the radial component with no/negligible energy on the transverse component, and a nearly linear initial particle motion. If there is slight noise on the transverse component but the particle motion is almost linear, it is a fair null. We only include good and fair nulls for further analyses. We measure splitting of shear waves in all frequencies as independent datasets, i.e., we do not require that a measurement be present in the low frequency to examine the waveform in the mid and high frequencies.

3.2 Layered Anisotropy

Shear wave splitting measurements are usually interpreted under the simple assumption of the waves sampling a single layer of anisotropy with a horizontal axis of symmetry (Silver & Savage, 1994). However, multiple studies have pointed out that this assumption is not always true (eg. Cherie et al., 2016; Dubé et al., 2020; Eakin & Long, 2013; Grund & Ritter, 2020; Liddell et al., 2017; Marson-Pidgeon & Savage, 2004; Savage & Silver, 1993). These studies have observed more complex nature of anisotropy which may be vertically-varying. Especially in regions like the eastern North America which have a long tectonic history with multiple deformation events, complex anisotropic structure is expected (eg. Aragon et al., 2017; Long et al., 2016). In the presence of complex anisotropy, the splitting directions and delay times vary systematically with respect to backazimuth of the waves (Alsina & Snieder, 1995; Rümpker & Silver, 1998; Silver & Savage, 1994). The 90° periodicity of fast directions and delay times with backazimuth is a typical evidence for the presence of at least two layers of horizontal anisotropy (Savage & Silver, 1993; Silver & Savage, 1994).

The most common method to model two-layered anisotropy is to use the characteristic relationship between changes in measured splitting parameters and backazimuth to perform grid search over a model parameter space to get the best-fitting values for fast directions and delay times for each layer (eg. Aragon et al., 2017; Cherie et al., 2016; Eakin & Long, 2013; Gao & Liu, 2009; Huang et al., 2017; Levin et al., 1999; Ritter et al., 2022). Following the method of Silver and Savage (1994), a grid search is performed over the model space consisting of the four splitting parameters (i.e., the upper- and lower-layer fast polarization directions and delay times). The grid search determines a best-fit model or a range of models that minimize the misfit between the observed and the expected apparent splitting parameters. The grid search procedure is non-unique and additional geological or geodynamic constraints are typically required (S. S. Gao & Liu, 2009; Kong et al., 2018; Walker et al., 2005). Nulls are not used to invert for the two-layer models but the null backazimuths can be used to evaluate model fit and compare whether it matches the expected null polarization (Y. Li et al., 2011; Ritter et al., 2022). Model fits are compared based on parameters like the misfit and the adjusted R^2 value (Abgarmi & Arda Özacar, 2017; Fontaine et al., 2007).

A major limitation using the approach of Silver and Savage (1994) is that sufficient backazimuthal coverage is required (Özalaybey & Savage, 1994). Having measurements from only a narrow band of backazimuths can bias the dataset and the modeling effort (Cherie et al., 2016). In order to detect the 90° periodicity exhibited by a dataset sampling multiple layers of anisotropy, it is required that splitting measurements be present over at least a 90° range of backazimuth (Cherie et al., 2016). This will not allow the identification of other potential scenarios of complex anisotropy such as dipping layers which exhibit 360° backazimuthal dependence (Liddell et al., 2017; Silver & Savage, 1994). Better backazimuthal coverage in event distribution is provided by the long-running stations which have more opportunity to record events originating from regions of lower seismicity (Figure 3.1). We inspect for the presence of a 90° periodicity in the splitting parameters versus backazimuth plot. If the station shows 90° periodicity, we require that the splitting dataset provide abundant coverage when we unwind and stack the dataset by transforming the backazimuths to a modulo 90° form.

We use the M-Split software package by Abgarmi & Arda Özacar (2017) to perform the layered anisotropy modelling. The parameter space goes from -90° to +90° with 1° increments in fast orientations and 0 to 2 s with 0.1 s increments in delay times of individual layer. For every set of model parameters, the predicted apparent splitting parameters are determined using the equations from Silver and Savage (1994). The predicted and the observed values are compared by calculating misfit based on either the unweighted, the weighted or the band-fit approach (Abgarmi & Arda Özacar, 2017). The model with the minimum amount of misfit is taken as the best-fit model. In the unweighted method, each observation has an equal influence on determining the final model. The weighted method provided more weighting to measurements with smaller errors. The band-fit method considers a predicted value to be fit (i.e., misfit = 0) by the observed value if their difference is within the error range of that individual observation. We choose to provide equal weighting to each individual measurement (Kong et al., 2018; Ritter et al., 2022) and therefore use the unweighted method for misfit calculation. The adjusted R^2 gives a measure of how much better the two-layer model output from the modeling attempt is than the best-fit single-layer model.

The grid-search procedure and hence the output models are inherently non-unique (Abgarmi & Arda Özacar, 2017; S. S. Gao & Liu, 2009). In order to deal with the non-uniqueness in these layered anisotropy modeling attempts, geological constraints such as the orientation of surface geological features like mountain belts as well as geodynamic constraints such as the direction of plate motion or mantle flow, are utilized to discriminate between possible suites of results (e.g., Eakin & Long, 2013; Levin et al., 1999; Polet & Kanamori, 2002; Wirth & Long, 2010).

Chapter 4

RESULTS

We obtained a total of 4238 individual spitting measurements (Figure 4.1, 4.2) with 2864 nulls and 1374 non-null measurements across all three frequencies. The low frequency has the highest number of measurements (i.e., 2348), followed by the mid frequency (1510) and the high frequency (380). The significant number of measurements in the low frequency is due to the preponderance of nulls (Figure 4.3). We obtained 2166 nulls in the low frequency, 619 in the mid and 79 in the high. The mid frequency has the majority of the splits (891) made in this study, followed by the high frequency (301) and the low frequency (182). In all three frequencies, most of the observed splits are measured on the SKS phase, followed by PKS and SKKS phases, respectively. The high frequency, even though having much less measurements (~9% of the total), is comprised of mostly splits. 301 out of 380 total (i.e., 80%) measurements in the high frequency are splits. There is a clear increase in the number of splits in stations near the Appalachian Mountains in all the frequencies (Figure 4.3). The average splitting direction changes spatially (Figure 4.4). The average delay time varies from 1.2 s in the low to 0.9 s in the mid and 0.6 s in the high frequency. There are multiple events that produce nulls in the low but exhibit splitting in the higher frequencies at the same station (Figure 4.1).

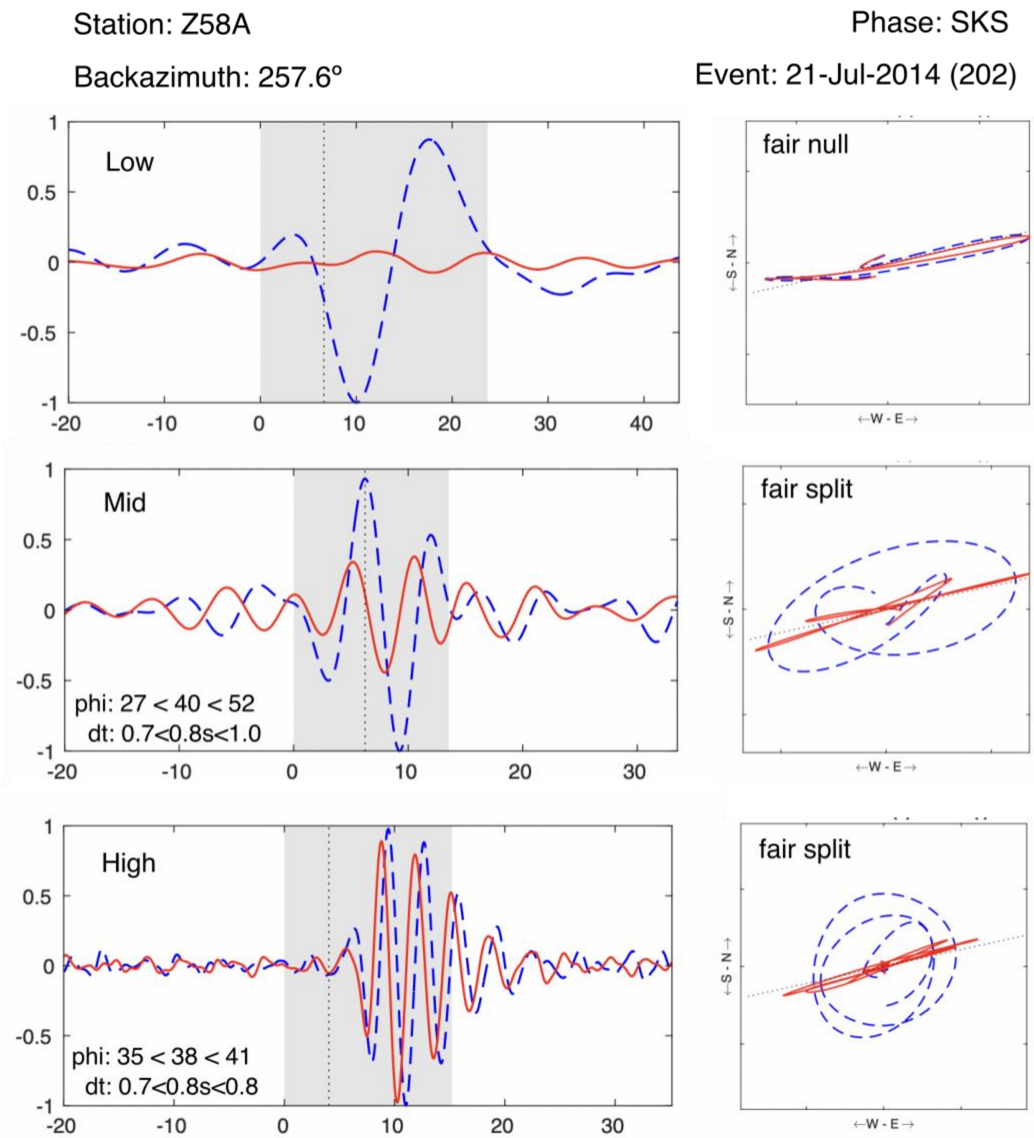

Figure 4.1 A single event producing measurements in all three frequencies in the same station. Left panels show seismograms SKS arrival in low, mid, and high frequency from top to bottom. Right panels show initial particle motion (dashed blue) and corrected particle motion (solid red) for the minimum energy method. Note the change in splitting behavior as the waveform appears null in the low frequency but yields similar splitting direction (ϕ) and delay time (dt) in the mid and the high frequencies.

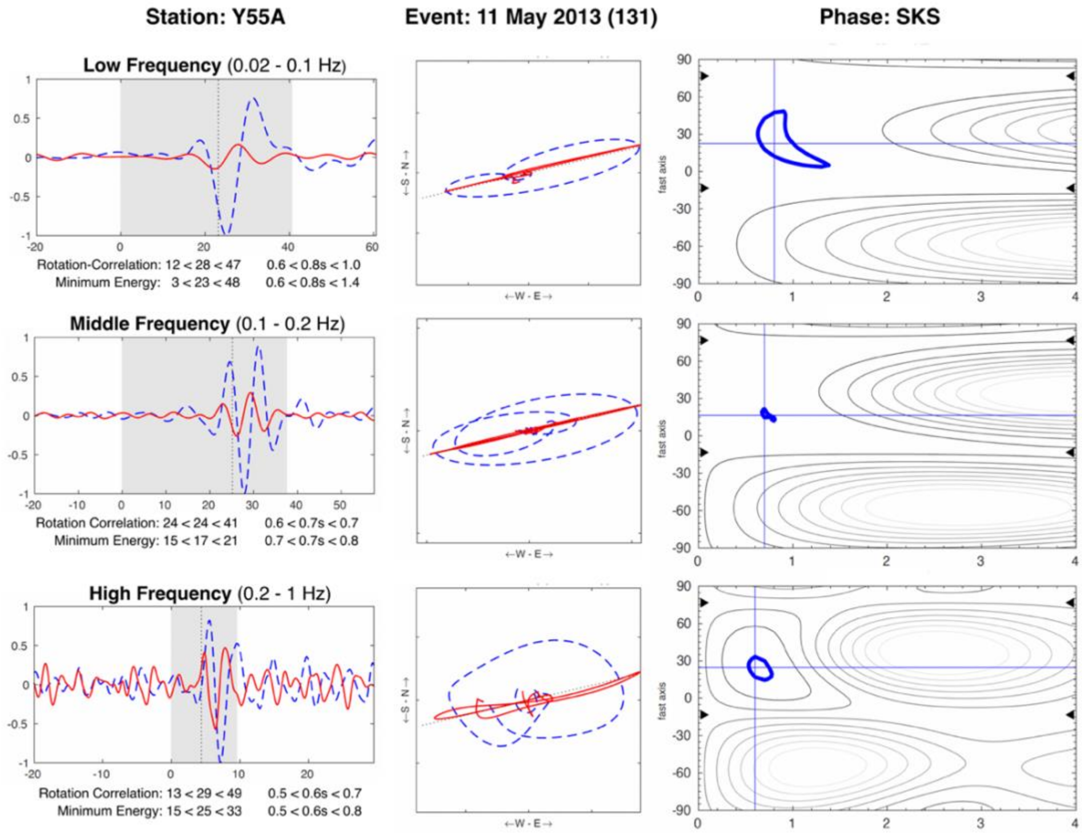

Figure 4.2 A single event yielding consistent splits in all three frequencies at the same station. **Left panels:** Seismogram showing SKS arrival in each frequency. **Middle panels:** Initial particle motion (dashed blue) and corrected particle motion (solid red) for the minimum energy method. **Right panels:** Error surfaces with 95% confidence region highlighted in blue for the minimum energy method. Station Y55A is located near the Carolinia Magnetic Lineament (CML). The fast directions for all three splits are ~NNE-SSW, similar to the trend of the CML near the station.

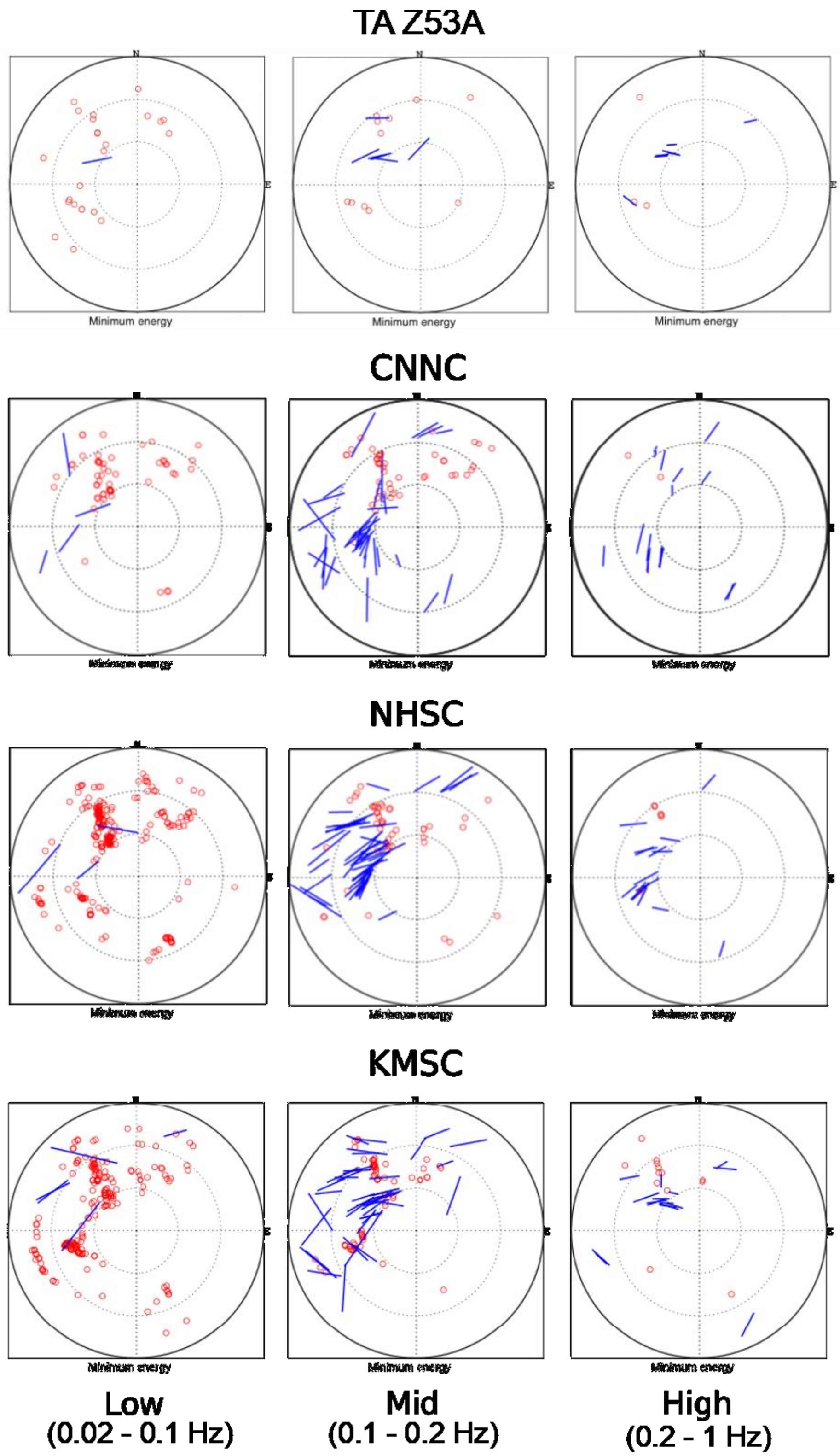
TA Z53A
Minimum energy
Minimum energy
Minimum energy
CNNC
NHSC
KMSC
Low
(0.02 - 0.1 Hz)
Mid
(0.1 - 0.2 Hz)
High
(0.2 - 1 Hz)

Figure 4.3 Stereoplots showing splitting patterns across low, mid, and high frequencies at a TA (Z53A) and three long-run stations (CNNC, NHSC and KMSC). Individual nulls (circles with red outline) and splits (blue lines) are plotted with respect to backazimuth (angle from north) and the angle of incidence (distance from the center). The orientation of the blue line indicates fast direction and length indicates delay time. Measurements in the low frequency show dominance of nulls. Splitting patterns for mid and high frequencies show the change in fast direction across backazimuths. Note the high number of measurements at all three long-run stations.

Our seismic stations record events arriving dominantly from the north-western and western backazimuths (Figure 3.1). There are smaller clusters of earthquakes from the northern and southern backazimuths. This is due to the concentration of seismicity at the subduction zones located at the western and southwestern Pacific. Due to this bias in event distribution, most of the measured splits have NW or W backazimuths. There is a clear gap in events coming from the east, especially in the TA and CSE stations. Owing to their longer life, the permanent stations KMSC, CNNC and NHSC have a better backazimuthal coverage and more measurements than the TA and CSE stations (Figure 3.1, 4.3). As a result, the permanent stations also have more total measurements than the TA and the ENAM-CSE stations in each frequency. However, in the low frequency data, there are several TA stations that yield a greater number of splits compared to the permanent stations.

4.1 Low Frequency

The low frequency data has a preponderance of nulls (Figure 4.3, 4.4). Among the 2348 measurements made in the low frequency band (10-50 s), 2166 (~90%) of them were nulls and 182 (~10%) were splits. This dominance of nulls over non-null splits holds true for all stations. There are 9 stations that produced only null measurements and 25 stations with nulls and only a single split. We interpret these stations as "null" stations in this study (Figure 4.5). Additionally, there are 7 stations with many null measurements and only 2 splits. We treat these stations as "near null" stations. There are several areas, however, such as near the Appalachian Mountains and in the coastal plain in southern North Carolina, where we observe strong splitting compared to the neighboring areas. In stations with splits, the station-averaged delay times range from 0.7 to 2.1 s.

We identify three dominant anisotropic regions based on the characteristics of the splitting parameters and the prevalence of nulls in the low frequency data: Orogen, East, and South (Figure 4.4). The north-west portion of our study area includes the Appalachian Orogen where the stations have lower number of nulls compared to the stations elsewhere. The 11 orogen stations yielded 47 splits (15%) and 260 nulls (85%). This region has one null and two near null stations. 8 out of 11 stations (72%) have more than 2 splits. The fast directions are consistently NE-SW, i.e., orogen-parallel with a regional average of 60° ± 20°. The average delay time is 1.2 ± 0.5 s. The null backazimuths are relatively well-constrained to be parallel or perpendicular to the fast directions of the splits.

The "east" region includes stations to the east of the Appalachian Mountains in North Carolina, and northern South Carolina and Georgia. There is a significant increase in the number of null measurements at individual stations (Figure 4.4). Most of the east stations are either nulls or near-nulls. The null backazimuths are not constrained to a narrow range and vary considerably. The 36 stations in the east yielded 118 splits (8%) and 1401 nulls (92%). The average delay time of the few split observations is 1.2 ± 0.5 s. The fast directions rotate from NE-SW just east of the

Appalachian Mountains to NNE-SSW near the coast. Between the orogen and the coast there is NE-SW splitting with more nulls than in the mountain stations. Despite having an overwhelming majority of nulls, there are two locations within the east that have a surprisingly high number of splits compared to the adjacent areas (Figure 4.4). The 4 stations in the Central Carolinas Region (CCR) have a consistent NE-SW fast splitting direction with a regional average of 57° ± 21°. The splits in the Carolinas Border Region (CBR) are oriented more NNE-SSW and have a regional average of 32° ± 20°. The 9 stations in CBR all have 1 s or more of delay times. Within CCR and CBR, all TA stations have >10% splits with some reaching up to 45% splits.

The southern part of our study area, near central Georgia and southern South Carolina, is also dominated by null and near null stations. This region produced the lowest number of split measurements. Only 2 out of 14 stations have >2 splits. From the 14 "south" stations, we obtained 16 non-null (3%) and 505 null (97%) measurements. The null backazimuths are not well-constrained. In contrast to the NE-SW fast polarizations further north, the splits are ~E-W oriented in the south region. The fast directions of splits change from ~ENE-WSW inland to more NE-SW and NNE-SSW towards the coast. The average delay time is 1.0 ± 0.4 s.

4.1.1 Low Frequency Results: Long-running Stations

The three long-run stations CNNC, KMSC and NHSC have more measurements than the average TA stations which have around ~20 measurements. Stations KMSC and NHSC have 214 and 249 measurements each, significantly more than any other stations. Despite having so many measurements, these long-run stations have <10% splits. Station KMSC just east of the Southern Appalachians has 2% splits. The average fast direction is NE-SW (66° ± 20°) with 1.3 s of average delay time.

This is similar to station NHSC in the coastal plain in South Carolina. Station CNNC along the coastal plain in North Carolina has 8% splits with average splitting parameters: 45° and 1 s. In contrast to the other two long-run stations, CNNC has only 60 measurements. In all three stations, there are nulls coming in from a wide range of backazimuths, but the fast directions of splits are constrained within a smaller range. Station CNNC has better constrained null backazimuths compared to NHSC even though both are along the coastal plain.

4.2 Mid Frequency

We obtained a total of 1510 measurements in the mid frequency band (5-10 s), among which 618 (~40%) were nulls and 891 (~60%) were splits. At most of the stations, we observe more split measurements than nulls (Figure 4.3, 4.4). The average delay time is 0.9 ± 0.2 s. All of the stations have multiple splits except one in eastern Georgia. Similar to the pattern observed in the low frequency, there are three distinct regions in the middle frequency splitting dataset. There is more scatter in the fast directions compared to the low frequency data, but the average error is lower (i.e., ±13°).

In the orogen stations (Figure 4.4, 4.5), we observed mostly NE-SW fast orientations with a regional average of 53°±11°. There are very few nulls and when present they are nearly parallel or perpendicular to the fast orientations. We obtained 155 splits (72%) and 59 nulls (28%) from the orogen stations. The average delay time is 1.0±0.2 s. To the east of the orogen, although we observe numerous splits, there is an increase in the number of nulls. From the east stations, we obtained 643 splits (57%) and 492 nulls (43%). The average fast polarization in the region is 47°±14° and the average delay time is 0.9±0.2 s. There is considerable variation in the fast orientations at these stations (Figure 4.4, 4.6). Some stations show multiple splits with nearly orthogonal fast directions. In general, the average splitting direction changes from NE-SW to NNE-SSW towards the shore. Following the CBR designated in the low frequency, there are several stations with relatively well-constrained N-S fast orientations (~30°) and fewer nulls. The stations in CBR have the highest proportion of splits among all stations in the mid frequency data, reaching up to 88%. All of the stations within CBR have >60% splits except CNNC. Within the CBR, a few of the stations have >1 s of delay time with the regional average being 1 s.

Stations in the south yielded 162 splits (57%) and 120 nulls (43%). Although variation is present, the general pattern shows ENE-WSW fast orientations that progressively change to NE-SW towards the coast. The average delay time is 0.8±0.2 s. Similar to the low frequency dataset, we observe a transitional region between the mountain and the eastern stations where the fast directions vary from almost E-W to NE-SW and there are more null measurements per station on average. The average delay times are higher near the Appalachians and near the North Carolina – South Carolina border.

4.2.1 Mid Frequency Results: Long-running Stations

All the long running stations (KMSC, CNNC and NHSC) have significantly higher number of measurements than the TA and the CSE stations in the mid frequency range. Station V56A is the TA station with the most measurements in this frequency band with a total of 35 observations: 22 splits and 13 nulls. CNNC has 81 measurements, NHSC has 96 and KMSC has 114. The percentage of splits in these stations is slightly lower than the regional percentage (57%): KMSC has 37% splits, CNNC has 46%, and NHSC has 52% splits. The delay times are similar with 0.9 s at

CNNC and ~1s at KMSC and NHSC. The average fast polarizations change from ~78° at KMSC near the Appalachians to ~44° at CNNC and ~62° at NHSC along the coastal plain. Although it has a lower proportion of splits, the fast directions at KMSC show significant scatter. At KMSC, we observe fast orientations covering the entire -90° to +90° range (Figure 4.3, 4.6). In contrast, most of the splits at CNNC and NHSC are constrained to a smaller range of fast directions. Systematic backazimuthal dependence of splitting parameters can be observed at all three long-run stations. Further, the plot of the splitting parameters at KMSC with backazimuth shows a clear 90° periodicity (Figure 4.6).

4.3 High Frequency

The high frequency yielded 380 measurements with 79 (~20%) nulls and 301 (80%) splits. The high frequency dataset has considerably lower number of nulls (70) compared to the low frequency (2166) and lower number of splits (301) compared to the mid frequency splitting (901) dataset. Even though the general pattern is that individual stations have more splits than nulls, there are 3 stations that yield only null measurements. 4 stations near the coastline did not produce any fair/good quality measurements. The station-averaged fast polarizations change laterally with an average error of ±11°. The average delay time among high frequency splits is 0.6 s ± 0.1 s.

We obtained 52 splits (84%) and (16%) nulls from the orogen stations. The average fast polarizations are oriented NE-SW, parallel to the Appalachian topography. The average delay time in the region is 0.6 s ± 0.1 s. Station V54A has the highest number of measurements (10 in total) in this region with 7 splits and 3 nulls. The east stations yielded 254 total measurements with 202 splits (~80%) and 52 nulls

(20%). Overall, the number of splits decreases towards the coast with 4 coastal stations yielding no useful measurements. The station-averaged fast direction changes from NE-SW just east of the mountains to ~N-S along the coast. There is more scatter in the stations adjacent to the mountains in western North Carolina, western South Carolina and northern Georgia. In the eastern part of the Carolinas, the fast directions are very consistently NNE-SSW. The average delay time for the east region is 0.6 s ± 0.1 s. At the southern stations, 64 total measurements were obtained. Among them, 47 (73%) are splits and 17 (27%) are nulls. The southern stations have fast orientations changing from ~E-W to more N-S as we go towards the shore. The average delay time for this region is similar to the orogen and the east regions, i.e., 0.6 s ± 0.1 s.

An additional observation from our study is the presence of robust splits in the high frequency data. Our high-frequency data with period between 1 to 5 s has a higher frequency band than the typical frequency ranges used in most shear wave splitting studies. For instance, the range of band-pass filters commonly used are: 2-25 s (S. S. Gao et al., 2008; S. S. Gao & Liu, 2009; Yang et al., 2017), 8-20 s (Fouch et al., 2000), 5-50 s (White-Gaynor & Nyblade, 2017b), 8-50 s (Long et al., 2016), and 10-50 s (Wagner et al., 2012). The 1-5 s period range exhibits higher degrees of contaminating noise due to contributions from large peaks in the Earth's microseism. Despite this noise, the average errors in fast direction (±11°) and in delay time (±0.1 s) are lower than the average errors in the low (±20°, 0.5 s) and the mid (±13°, 0.2 s).

While the overall number of splits in the high frequency data is a third of that seen in the mid frequency, this decrease in observations is not uniform and is far more pronounced near the coast. The number of high-frequency measurements decreases from ~10 at TA stations near the mountains to none at the coastal ENAM-CSE stations. This correlates well with the expectation of higher levels of noise along the shoreline. In the near-coastal region, short-period secondary microseism with period <5s is produced by wave interactions (Bromirski et al., 2005). The coastal ENAM-CSE stations, having greater proximity to the shoreline, have noisier data compared to the stations located further inland at the Appalachian Mountains. Further, site conditions at coastal stations differ from the orogen stations which are more likely to be placed on bedrock or over thin residual soil covering the rock outcrops (Z. Guo & Chapman, 2019). The higher sediment thickness at the coastal stations corresponds to the higher attenuation of high frequency waves (Z. Guo & Chapman, 2019), leading to poor data quality at these stations in the high frequency range. Well-resolved splits exist at most stations in the high frequency band despite the higher levels of noise compared to the mid and the low frequencies, but the yield is very sensitive to data quality issues.

4.3.1 High frequency results: Long-running stations

All long-run stations have higher number of measurements than the TA and CSE stations although the difference is not as high as in the mid frequency data. Station CNNC has 16 total measurements with 13 splits (81%) and 3 nulls. For reference, the highest number of measurements in the high frequency data at TA stations is 12. Station KMSC has 34 total data points with 19 splits (56%) and station NHSC has 24 observations with 17 splits (71%). The fast directions at KMSC have more scatter compared to the fast directions at CNNC and NHSC. This pattern is similar to what we observed in the mid frequency data. The average delay times are similar for all three stations: CNNC = 0.5 s, KMSC = 0.5 s, and NHSC = 0.6 s.

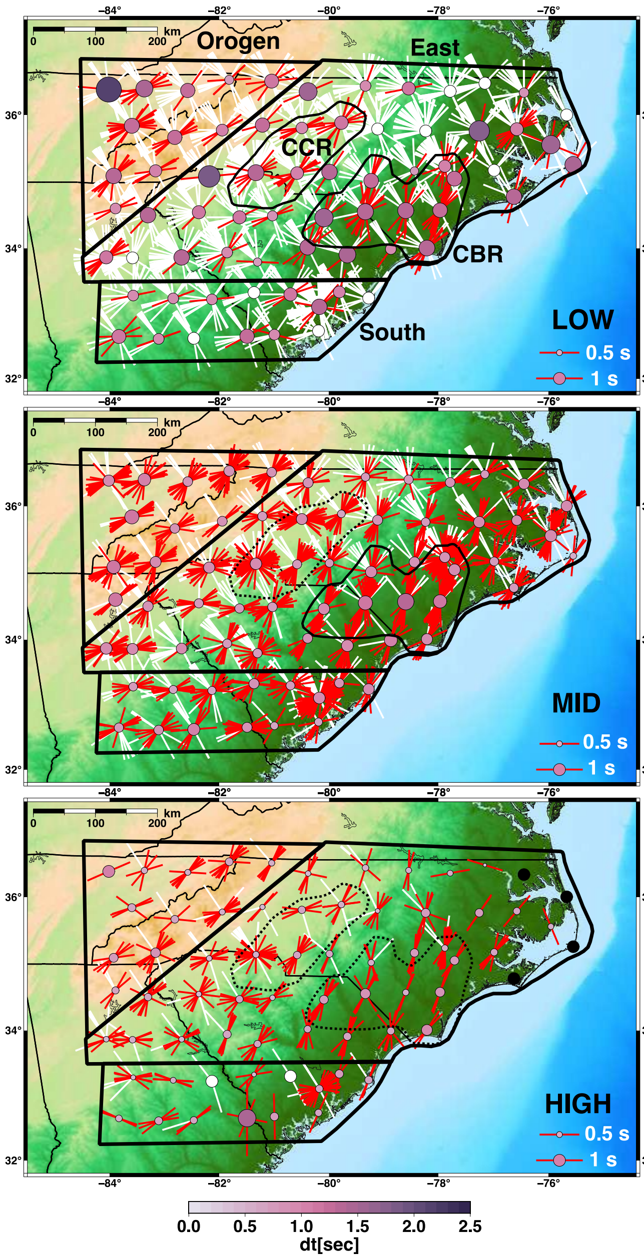

Figure 4.4 Individual splitting measurements in low, mid, and high frequencies from the study area. Red lines are oriented parallel to splitting fast directions and scaled according to delay times from the minimum energy method. Each circle corresponds to a station. The color and size of the circles denote average delay time at each station. White lines give backazimuths of nulls. Note the dominance of nulls in low frequency and abundance of splits in mid and high frequencies. Thick black solid lines delineate the three major splitting domains: Orogen, East and South. Regions

designated by thinner black lines in the low frequency results represent areas with stronger splitting: at central North Carolina and South Carolina, there is the Central Carolinas Region (CCR) and near the coast there is the Carolinas Border Region (CBR). In the mid frequency, CBR persists as a region of slightly higher delay times. CCR in the mid and both CCR and CBR in the high frequencies are not conspicuous and are delineated by dotted lines.

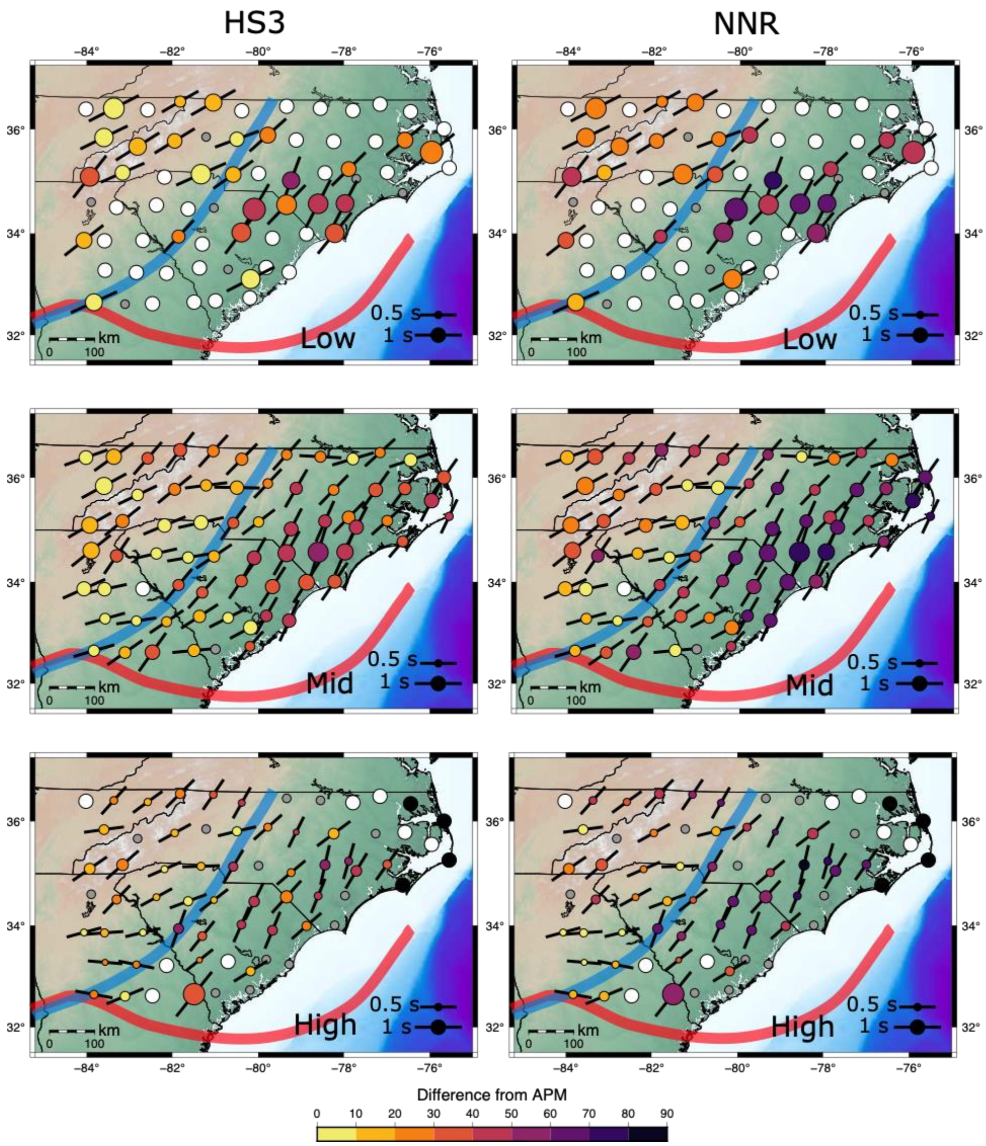

Figure 4.5 Splitting averages for each frequency compared to the North American plate motion. The low-, mid- and high-frequency splitting parameters are

shown from the top to the bottom panels respectively. The black line at each station represents the average fast direction. The lengths of the lines as well as the size of the circles are proportional to the average delay times. Left panel shows the deviation of station-averaged fast directions with respect to the hotspot reference frame (HS3-NUVEL1A: Gripp & Gordon, 2002) and right panel shows the deviation in no net-rotation reference frame (NNR-MORVEL56: Argus et al., 2011). Blue line shows the approximate trace of the Carolinia Magnetic Lineament (CML) (Hatcher, 2010) and red line shows that of the Brunswick Magnetic Anomaly (BMA) (Parker, 2014). White circles are null stations and grey circles are near-null stations. Splitting averages are shown only for stations with 3 or more splits.

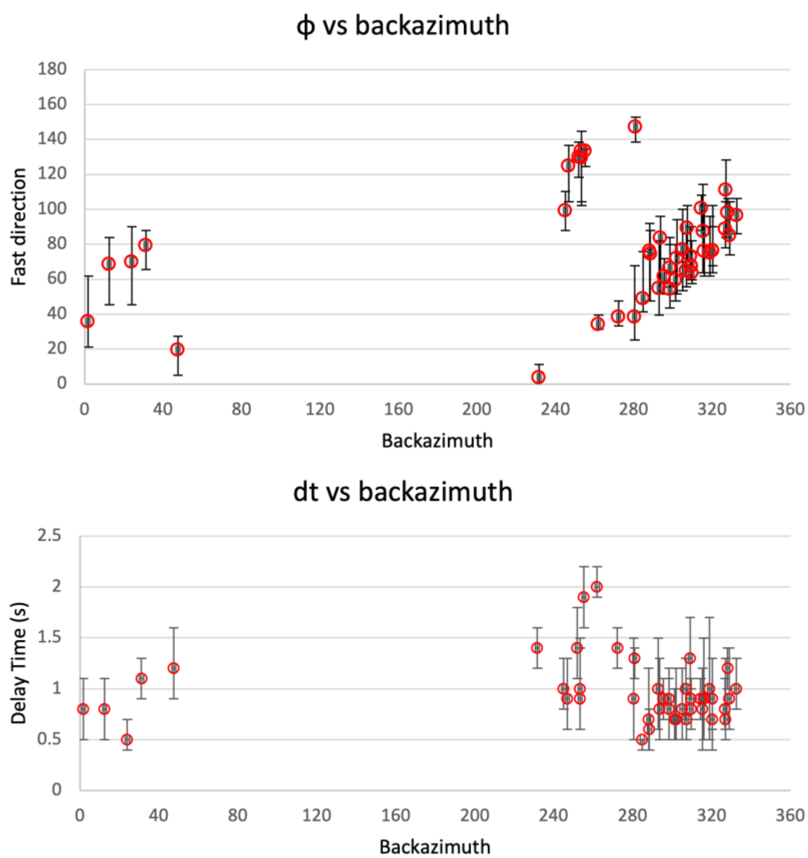

Figure 4.6 Backazimuthal variation of splitting parameters: ϕ and dt in the middle frequency measurements at station KMSC. Note the clear 90° periodicity in fast directions with incoming backazimuth.

4.4 Variation of Splitting Parameters across Frequencies and Lateral Regions

The proportion of splits increases from the low- (10%) to the mid- (60%) to the high- (80%) frequency dataset. Regions that are dominated by nulls in the low frequency yield abundant splits in the higher frequencies. In all three frequencies, three major regions: orogen, east and south, can be identified based on the splitting patterns and the null measurements (Figure 4.7). The average delay time decreases with increasing frequency but is still above the 0.5 s threshold for detection of splitting in the low frequency band (Long et al., 2016; Long & Silver, 2009). The average errors in splitting parameters decrease from ±20° , ±0.5 s in the low frequency to ±13° , 0.2 s in the mid frequency and ±11° , ±0.1 s in the high frequency. Although the average fast polarizations do not vary significantly across frequencies, there are some regions where we observe a change.

Near the Appalachian Orogen, we observe a consistent NE-SW fast orientation in all three frequencies. To the east, there are dominantly null and near-null stations in the low frequency data with strong splitting signal from two specific regions in the Carolinas: the CCR and the CBR. In the mid frequency, there are no null stations and only a single near-null station. At CCR stations, the NE-SW fast directions that we observed in the low persist in the mid but there is more variation. All four CCR stations have coherent NE-SW station-averaged fast orientations in the low frequency. At the two western CCR stations, the fast directions rotate towards an E-W orientation whereas they rotate more towards N-S at the two eastern stations in both the mid and the high frequencies. This change in the splitting pattern can be further traced to the north and south of CCR in the mid and the high frequencies. At CBR stations, the splitting directions in the mid is ~N-S, consistent with that in the low, and several stations have a higher station-averaged delay time than the adjacent regions. A distinct splitting signal from the CBR can be observed in the mid frequency. Broadly, the station-averaged fast directions in the high frequency data are approximately the same as that in the mid. The CCR and the CBR cannot be identified distinctly in the high frequency data. An interesting observation in the high frequency is that we see a clear change in the splitting behavior from more scattered fast directions just east of the mountains in western Carolinas and northern Georgia to more coherent fast directions along the eastern Carolinas. The spatial occurrence of this change coincides with the change in station-averaged splitting directions from more E-W to more N-S across the CCR in both the mid and the high frequencies.

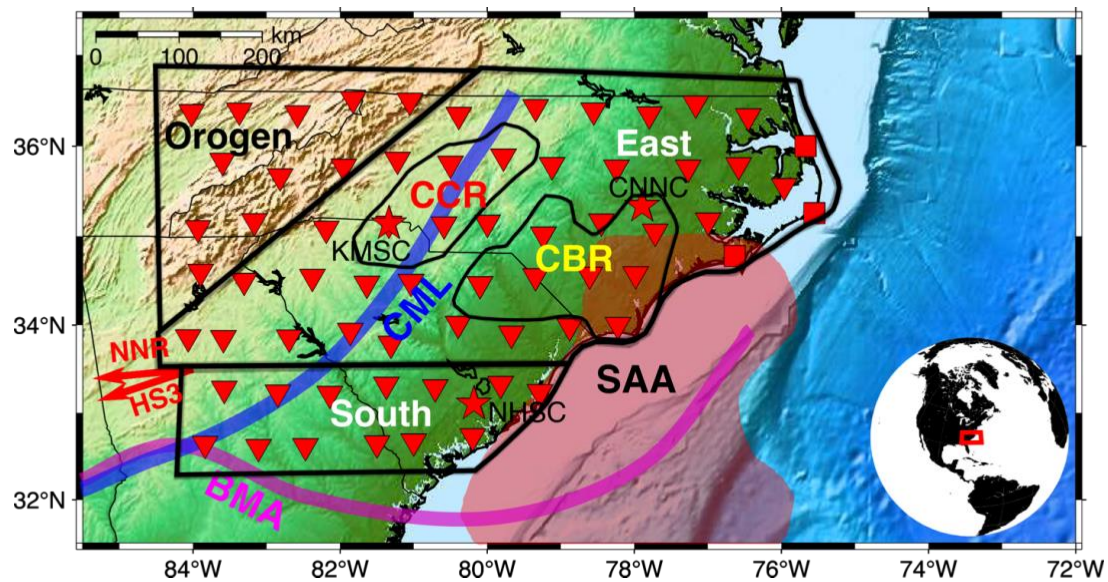

Figure 4.7 Three main splitting domains identified based on the observations across the low, mid and the high frequencies: Orogen, East and South. In the east domain, two localized regions with distinct splitting pattern: the Central Carolinas Region (CCR) and Carolinas Border Region (CBR) are present in the low frequency. CBR can be identified in the mid frequency as well. Note the proximity of CBR to the low-velocity anomaly, SAA (B. Savage et al., 2017).

In the southern part of the study area, the pattern of null stations dominating the low frequency and yielding abundant splits in the mid and the high frequencies still holds true. We observe a change in the average splitting directions from NE-SW or ENE-WSW in the low and the mid to more ESW-WNE in central Georgia. Along the coast, however, stations have either consistent NE-SW or N-S fast polarization in the mid and the high frequencies. These observations point to the presence of frequency-dependent splitting beneath the east coast.

Chapter 5

DISCUSSIONS

5.1 Frequency Dependence of Splitting Parameters and Comparison with Previous Studies

The change in splitting behavior across the frequencies (Figure 4.1, 4.3, 4.4) with predominantly nulls in the low frequency and significant amount of splitting in the mid and high frequencies point to the frequency-dependent nature of splitting in our study region. Frequency dependence is observed in regions with complex anisotropic structures arising from vertically-varying anisotropy (Rümpker et al., 1999; Rümpker & Ryberg, 2000; Rümpker & Silver, 1998). Along the eastern margin, depth-dependent anisotropy is plausible due to expectations of having both lithospheric and asthenospheric sources of anisotropy. Lithospheric anisotropy is potentially related to collisional deformation during the formation of Pangaea or rift-related deformation during its break-up (e.g., Brunsvik et al., 2021; Long et al., 2016). Plate motion-induced or edge-driven convection associated anisotropy is likely driving patterns in the asthenosphere (e.g., Brunsvik et al., 2021; Long et al., 2016; Yang et al., 2017; Yuan & Romanowicz, 2010). Anisotropic fabrics appear to change from the mountains to the coast, so there may be some contribution of lateral heterogeneities to frequency dependence as well. However, the splitting parameters at many adjacent stations do not vary significantly. This suggests that the observed frequency dependence is unlikely to be driven by small-scale lateral heterogeneities.

Higher frequencies are more sensitive to thinner anisotropic features (Long & Silver, 2009; Saltzer et al., 2000). One of the most important observations in this study is the prominence of null regions to the east and south-east of the Appalachian Mountains in the low frequency which subsequently produce splits in the mid and the high frequencies. This suggests the presence of a thin enough layer such that the long periods miss the anisotropic signal present in the mid and the high frequencies at a station (Figure 4.1). This layer may be either in the lithosphere or in the asthenosphere. The nulls in the low frequency could be sampling a thicker layer that has anisotropy with vertical fast axis. In regions where we observe splitting in all three frequency bands with near-consistent fast directions like the Appalachian Mountains and in southern North Carolina at the CBR, it is more likely that a single, thicker layer of anisotropy is present. In other regions where the low frequency yields mostly nulls and the mid and the high yield splits but with larger variation in the splitting fast directions across frequencies such as at the CCR, layered anisotropy with different anisotropic geometry is more likely.

The change in the splitting behavior laterally from the mountains to the coast is made more evident by examining the three long-run stations (Figure 4.3). The permanent stations yield significantly more splits in the mid frequency than the TA stations. This extra data coverage allows us to further probe the nature of anisotropy beneath the stations. At station KMSC, the low frequency exhibited only 5 total splits that were constrained to a relatively narrow range of NE-SW azimuths and made up a miniscule portion of the overall number of measurements (i.e., 2%). Additionally, several nulls were measured along the same backazimuth where those few splits originated. In the mid frequency, splitting becomes dominant over all backazimuths, and the fast orientations vary significantly. The fast directions span the entire -90° to +90° range and show a 90° periodicity suggesting vertically-varying anisotropy. Stations CNNC and NHSC along the coast have more consistent fast directions, showing lesser degrees of variation. All three permanent stations follow the general pattern of dominantly nulls in the low frequency, substantial number of splits in the mid frequency and more splits than nulls in the high frequency. However, the difference in the degree of variation of fast orientations implies that the anisotropic structure beneath the Appalachian region is different than that beneath the coast (Figure 4.3, 4.4).

Our splitting results from the low frequency match well with those observed by Long et al. (2016). There is dominance of null measurements along the coast. The two southern rows of stations in our dataset correspond to region D in Long et al. (2016) and have ~E-W fast directions in central Georgia to NE-SW and almost N-S fast directions in southeastern South Carolina, similar to the fast orientations previously observed. Additionally, we see similar fast directions in region C in Long et al. (2016) with mostly NE-SW fast axes which align with the Appalachian topography (Long et al., 2016). Conversely, the pattern of fast directions in our middle frequency measurements broadly matches that of Yang et al. (2017). We find multiple splits at all of the stations. Along the coast, the prominent margin-parallel (~N-S) fast anisotropic directions match well with the observations by Brunsvik et al. (2021), Liang et al. (2022), and Yang et al. (2017). However, contrary to smaller delay times along the coast observed by Yang et al. (2017), some of our coastal stations have ~1s of delay time. The discrepancy in the splitting observations between Long et al. (2016)

and Yang et al. (2017) can largely be attributed to the frequency-dependent nature of splitting along the ENAM.

5.2 Contributions from Different Sources of Anisotropy

Assuming a shear wave travelling at 4.5 km/s through the mantle with 4% anisotropy, a ~135 km thick layer is required to explain the 1.2 s of average delay time that we observe in the low frequency data (eg., Schmid et al., 2004; Silver, 1996). Similarly, the 0.9 s average delay time (dt) in the mid frequency would require ~100 km thick layer and the 0.6 s average dt in the high frequency would require ~65 km of layer thickness. Conversely, stronger anisotropy could yield these delay times even if the layer was thinner. This could explain why we see widespread nulls in the low but splits in the higher frequencies at most of the regions. Low frequency waves have reduced sensitivity to stronger anisotropic gradients (Rümpker et al., 1999) and therefore cannot effectively sample thinner anisotropic layers. In the Appalachians and at the CBR where we have coherent splitting in all three frequencies, a thicker anisotropic layer is more likely. Where we observe consistent fast directions, it is possible that the waves are sampling a single anisotropic layer, or at least what can be modeled as a single cohesive layer of anisotropy.

A common contributor to ≥1 s of delay time in continental settings is plate motion-induced CPO in the asthenosphere. The comparison of the station-averaged splitting fast polarizations at each frequency band with the plate motion of North America shows clear discrepancy between the two, most conspicuously around the eastern North Carolina-South Carolina border (Figure 4.5). Plate motion-induced CPO is not enough to explain the splitting patterns that we observe. In both the hotspot (Gripp & Gordon, 2002) and the no-net rotation (Argus et al., 2011) reference frames, the fast directions and the plate motion directions agree more around the Appalachian Mountains while the deviation to splitting increases along the coast. Between the two reference frames, the hotspot model, HS3-NUVEL1A by Gripp and Gordon (2002) provides a lower deviation and has been used previously in multiple studies to interpret splitting observations (eg., Long et al., 2016; Yang et al., 2017). We take the hotspot reference frame to represent the North American plate motion and compare it with our observed splitting fast directions.

At the Appalachian Mountains, the consistent NE-SW splitting across all three frequencies parallels both the Appalachian topography and the plate motion in hotspot reference frame. The lithosphere beneath the orogen is thick enough (~200 km) (van der Lee, 2002) to account for the ~1.2 s delay time observed here. There could be either a lithospheric or an asthenospheric contribution to the anisotropy beneath the mountains. As the fast directions expected from both sources are parallel, it could also mean that we have both lithospheric and asthenospheric contributions. This would mean that deformation related to the formation of Pangaea is still preserved in the Appalachian lithosphere.

East of the Appalachians, the preponderance of null stations in the low frequency suggests the anisotropic signal along the coastal plain is not as strong as that in the mountains. However, the presence of multiple splits (although <50%) even in the low frequency and ~1 s of dt at CCR and CBR point to lateral changes in anisotropic structure. At the CBR, the fast polarizations are persistently ~N-S (margin-parallel) in all frequencies. The average dt is higher than at adjacent regions in the low and the mid frequencies. The null backazimuths are better constrained compared to the stations to the north and the south in the low frequency. The waves arriving at these stations are sampling a thicker or stronger anisotropic layer. This could be in the asthenosphere due to margin-parallel flow generated by 3D edge-driven convection (EDC) (Kaislaniemi & van Hunen, 2014; King & Anderson, 1998; Yang et al., 2017). A low velocity anomaly observed near the coastal region of South Carolina has been interpreted as an upwelling limb of an edge-driven convection cell (B. Savage et al., 2017). This could mean that at CBR there is more vigorous mantle flow associated with the EDC upwelling leading to larger strains, more coherent anisotropic fabrics, and hence stronger splitting.

Alternately, there could be N-S aligned anisotropy frozen-in in the lithosphere at CBR. This anisotropic geometry could be related to paleo-plate motion after the Appalachian orogenesis (Deschamps et al., 2008). While paleo-plate motion parallel anisotropy has been invoked for offshore parts of the margin where new lithosphere forms with spreading (Russell & Gaherty, 2021), why it would be preserved in the continental lithosphere needs further study. It is also unclear why only some parts of the margin would preserve this N-S aligned anisotropy in the lithosphere. Although rift-parallel anisotropy has been observed in modern rifts, this is due to shaped-preferred orientation of melt lenses (Kendall et al., 2005, 2006). At mature passive margins, the solidified melts would not have a significant seismic velocity contrast with the surrounding rocks (Brunsvik et al., 2021). It is also possible that N-S aligned anisotropy exists in both the lithosphere and the asthenosphere beneath the CBR and is responsible for strengthening the splitting signal.

At the Central Carolinas Region (CCR), multiple splits present in the low frequency reflect a stronger splitting signal even though the proportion of splits does not exceed 25%. The null backazimuths are more scattered compared to the stations in

CBR. The coherent NE-SW average fast directions in the low frequency changes to more E-W fast direction to the west and more N-S fast directions to the east across the CCR in the mid and the high frequencies. This pattern of change can be traced further south in both of the higher frequencies and occurs across the Carolinia Magnetic Lineament (CML). The average fast directions follow the trend of the CML where stations are located near the lineament (Figure 4.2, 4.5), citing some lithospheric contribution associated with past suturing events (Long et al., 2016; Wagner et al., 2012). At the long-run station KMSC in the CCR, the 90° periodicity in fast directions suggests the presence of at least two layers of anisotropy.

The prevalence of null stations in the low frequency in central Georgia and southern South Carolina contrasts the numerous splits observed in the higher frequencies. The anisotropy beneath this southern part of our study area could be weaker or constrained to a thinner layer. The mid frequency splits seem to somewhat but not perfectly align with the plate motion, invoking some contribution from asthenospheric flow due to simple shear at the base of the lithosphere. The fast directions in the high frequency have more deviation and might be associated with lithospheric anisotropy. A few stations in central Georgia emulate the ESE-WNW trend of the Brunswick Magnetic Anomaly (BMA) although this correlation is unclear towards the coast. The "south" region is located between the Suwanee Suture in the north and the BMA in the south and likely exhibits anisotropy related to the suturing of accreted terranes (Mueller et al., 2014; Parker, 2014).

The coastal plain to the east and south-east of the Appalachians being populated by null stations in the low frequency argues for a thick layer with weak/no anisotropy or a vertical axis of anisotropy and a thin anisotropic layer. Our low frequency results alone, however, do not provide sufficient evidence to confidently distinguish between the above hypotheses. When interpreted with results from the mid and high frequency splitting, we see that anisotropy is present over the entire margin, but the low frequency waves are not effectively sampling it. Besides strong anisotropy being present in a thinner layer, it is also possible that there is vertical flow over most of the asthenospheric mantle beneath the null regions. The vertical flow component could be related to the downwelling or upwelling limbs of edge-driven convection (King & Anderson, 1998; King & Ritsema, 2000) or shear-driven upwelling (e.g., Brunsvik et al., 2021; Long et al., 2021). This interpretation of vertical flow ties well the null observations in the low frequency dataset and the low-velocity anomalies reported in previous tomography results.

5.3 Layered Anisotropy Modeling

Our observation of frequency-dependent splitting suggests vertically-varying anisotropy beneath the study area. To further test this, we perform layered modeling at the permanent stations. We do not model the splits at the temporary TA stations because measurements are limited to a narrow backazimuthal ranges. The low frequency results are dominated by nulls at all three long running stations. In the high frequency data, splitting is clearly present, but measurements are relatively sparce due to noise issues. Our high frequency range (1-5 s) is noisier because of short-period microseisms. Therefore, only the mid frequency provides a better dataset for the modeling efforts. Each of the permanent stations have at least 10 years of data, with NHSC having the most at 21 years of data. The splits measured at each stations cover greater than a 90° range of backazimuth, which is necessary to distinguish the case of multi-layered anisotropy.

A plot of the splitting patterns at the three permanent US network stations shows backazimuthal dependence (Figure 4.3, 5.1, 5.2, 5.3). However, only station KMSC shows a clear 90° periodicity in fast directions (Figure 4.6). Even though there are no splits coming from the southeast quadrant, KMSC has enough backazimuthal coverage to model layered anisotropy. Our best-fitting two-layer model, M1, (Figure 5.1) is based on the unweighted approach (Abgarmi & Arda Özacar, 2017) has upper layer splitting parameters: 81°, 0.8 s, and lower layer splitting parameters: 54°, 0.2 s with misfit = 40.15. The adjusted R^2 for this model is 0.73. The best-fit single layer model for the mid frequency measurements at KMSC has fast splitting direction = 30°, delay time = 1s and misfit = 157.49. Based on the misfit values, the two-layer model provides a better fit than the single layer best-fit. We also performed layered modeling using the weighted and the band-fit approach of Abgarmi & Arda Özacar (2017). Although there is a lot of variation among these models, a common feature of the top 15 best-fit models is that there is a significant contribution of 0.8 to 1.8 s from a layer with orientation between 71° to 81°. In some models, this is the top and in others the bottom layer. This fast orientation is within 10° of the expected plate motion at KMSC which is S71°W in the hotspot reference frame (Gripp & Gordon, 2002).

In our best-fit model, the upper layer (81°, 0.8 s) could be a layer in the lithosphere or in the asthenosphere. The upper layer splitting fast direction is within 10° of the plate motion at KMSC. The lower layer (54°, 0.2 s) could be a modified component of mantle flow related to small-scale convection along the edge. Alternatively, the upper layer has fast directions close to margin-perpendicular and the lower layer is more margin-parallel. This is similar to the layered anisotropic structure observed in western South Carolina by Brunsvik et al. (2021), who interpreted it as extension-parallel lithospheric anisotropy over margin-parallel asthenospheric flow. It is also possible that there are three layers of anisotropy in this region with frozen-in lithospheric anisotropy, APM-parallel asthenospheric layer and a layer with flow modified due to edge-driven convection.

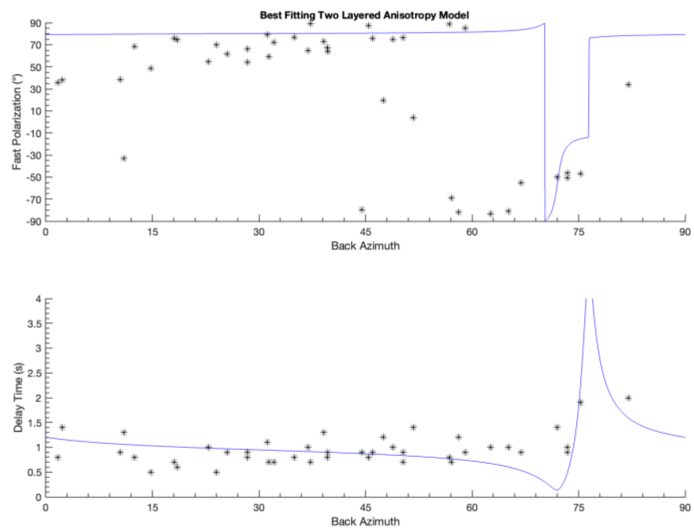

Figure 5.1 Curves for the best-fit two-layer model using the unweighted approach at station KMSC using splits from the mid frequency measurements. The fast directions show a clear 90° periodicity with backazimuth. The best-fit model does not explain all the variations in the data.

At stations CNNC and NHSC, there is some backazimuthal variation in fast direction, but the delay times seem to be constant (Figure 5.2 and 5.3). Our modeling results for both stations have fast directions within 10° to 20° between the layers, suggesting that even though layered anisotropy resulting in frequency dependence is present beneath these stations, the orientations of the fast axis in these layers are similar enough to be considered a single layer of anisotropy.

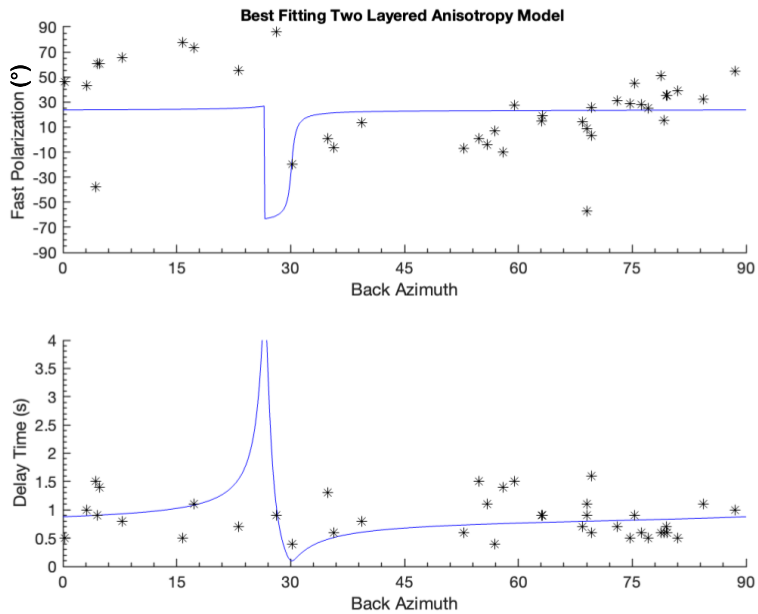

Figure 5.2 Same as 5.1 but for station CNNC.

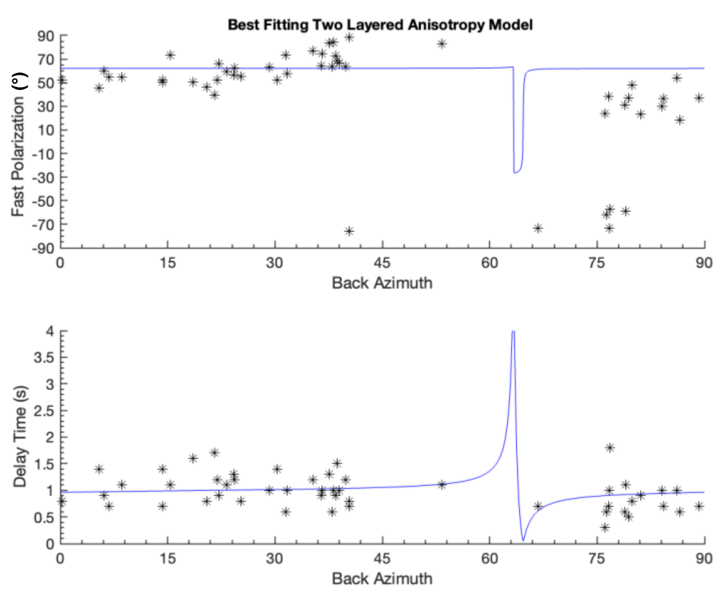

Figure 5.3 Same as 5.1 but for station NHSC.

5.4 A Preferred Model: Implications for Past Deformation and Current Dynamics

Our preferred model (Figure 5.4) has anisotropy changing with depth as well as laterally from the orogen to the coast. The significant change in the proportion of nulls and splits with increasing frequency invokes depth-dependent anisotropy in the study region. The dominance of null stations in the low frequency data suggests the presence of an anisotropic layer with vertical fast axis beneath most of the coastal plain. Despite being predominantly null, the presence of localized regions of coherent splitting in the low frequency warrants spatial variation in the nature or strength of anisotropy. The abundance of splits in the mid and the high frequencies in contrast to the nulls in the low is due to the presence of a relatively thin layer that the low frequency is not sensitive to. Some regions, however, have persistent splits in all frequencies that are either due to a singular thick layer or due to multiple layers that have similar anisotropic geometry. The single layer or the multiple layers could be either lithospheric, asthenospheric, or both and this provenance likely changes laterally across the margin. A dominantly lithospheric contribution beneath the Appalachian Mountains and a significant asthenospheric contribution along the coast better explains the observed splitting patterns.

Beneath the Appalachians, we interpret a significant lithospheric contribution owing to the correspondence of average fast directions with the Appalachian topography at each frequency. The lithosphere beneath the mountains is thick enough (~200 km (Yuan et al., 2011)) to produce the 1.2 s delay time observed in the low frequency. As the coherent NE-SW splitting at the mountains is also parallel to plate motion, there might be an additional asthenospheric flow contribution. However, this agreement is only strong in the hotspot reference frame and becomes weaker if we consider the no-net rotation frame. At individual stations, the fast directions deviate more from the plate motion with increasing frequency but the agreement with the trend of the orogen remains (Figure 4.5).

Along the coast at the North Carolina-South Carolina border, we argue for a primarily asthenospheric contribution. The consistent ~N-S fast directions in all frequencies with >1 s of splitting in the low frequency needs contributions from the asthenospheric mantle as the lithosphere thins out to <150 km (H. Gao & Li, 2021) beneath the coastal plain. The margin-parallel shear wave splitting could be due to keel-deflected flow (Fouch et al., 2000) or flow modified due to edge-driven convection (Kaislaniemi & van Hunen, 2014; King & Anderson, 1998). The N-S fast directions correspond well to the possible margin-parallel component of edge-driven convection in three-dimension (Kaislaniemi & van Hunen, 2014). The low-velocity anomaly near South Carolina, either inland (Biryol et al., 2016) or offshore (Brunsvik et al., 2021; B. Savage et al., 2017), could be an upwelling related to edge-driven convection. The presence of an upwelling limb adjacent to the CBR could mean larger strains producing stronger, more coherent anisotropy at this region. This also explains why there are higher delay times at the CBR in the low and mid frequencies compared to the adjacent regions. Our interpretation agrees with the observation of margin-parallel anisotropy at asthenospheric depths by Brunsvik et al. (2021) and Liang et al. (2022).

As the splitting fast directions are consistently similar in all three frequencies around CBR, lithospheric anisotropy, if present, should be N-S aligned as well. CPO-induced due to North American plate motion during spreading as proposed offshore (Russell & Gaherty, 2021) is less likely for the continental part of the margin. As new lithosphere forms in the oceans, the paleo-plate motion-induced CPO is possible there. However, in the continental part, the pre-existing lithosphere is deformed. Pre-rift collisional orogen-parallel fabric could be present in the coastal lithosphere but has likely been overprinted by the Mesozoic rifting (e.g., Aragon et al., 2017; White-Gaynor & Nyblade, 2017). SPO due to aligned melt could produce a rift-parallel (therefore, margin-parallel) fabric. However, SPO alone likely cannot result in the ~1 s delay times that we see as the melt is solidified at mature margins and the velocity contrast becomes minimal. Margin-parallel anisotropy could be present in the lithosphere beneath the coast, but the asthenospheric contribution is more prominent.

Most areas to the east and south-east of the mountains where nulls are dominant in the low frequency can be explained by the presence of a vertical flow component in the asthenosphere. The splits in the higher frequencies reject the possibility of weak or no anisotropy. There is no considerable change in splitting fast direction across frequencies ruling out multiple anisotropic layers that cancel each other. Our interpretation of vertical mantle flow agrees with the observation of low-velocity anomalies along the coast (e.g., Biryol et al., 2016). These anomalies are considered to be mantle upwellings related to edge-driven convection, shear-driven upwelling or return-flow associated with lithospheric delamination (Biryol et al., 2016; Brunsvik et al., 2021; B. Savage et al., 2017). Although we cannot discern the cause of the upwelling, our observation of margin-parallel flow follows the pattern expected from edge-driven convection.

The splitting, abundant in the mid and the high frequencies, in the regions designated as nulls in the low means that a thin anisotropic layer is present either in the lithosphere or the asthenosphere (Figure 4.1). In Georgia and the western

Carolinas, the change in station-average fast directions across the Carolinia Magnetic Lineament (CML) calls for a significant lithospheric contribution. Similar to Long et al. (2016) and Wagner et al. (2018), we observe fast splitting orientations parallel to the CML. This might be associated with the frozen-in fabric from past terrane accretion of the Inner Piedmont and the Carolina superterrane (Hatcher, 2010). The presence of lithospheric anisotropy along the CML is supported by lineament-parallel splitting in the mid- and the high-frequency. The localized stronger splitting at CCR could either be due to stronger lithospheric anisotropy or constructive contributions from the lithosphere and the asthenosphere. As the lithosphere beneath the CCR is relatively thicker than beneath the coast, it is possible that the anisotropy is mostly lithospheric. However, we have null stations to the north and south of CCR in the low frequency. The CML passes through this region and the lithospheric thickness is similar to that at CCR as indicated by the uniform shear velocity anomaly in the model by Porritt et al. (2021) shown in Figure 1.1. A similar anisotropic fast direction in the asthenosphere that is strengthening the lithospheric signal might explain this pattern better.

Although less pronounced than the CML, there is some lithospheric anisotropy associated with the Brunswick Magnetic Anomaly (BMA) near central Georgia. The splits which are more aligned with plate motion in the mid frequency rotate to a more E-W orientation in the high frequency. This splitting could either be related to deformation during the Alleghenian convergence (Parker, 2014) or the rifting of Pangaea (Duff & Kellogg, 2019). As the stations spatially far from the BMA still produce E-W splits in the high, it is more likely due to extension-parallel frozen-in anisotropy (Tommasi et al., 1999; Vauchez et al., 2000).

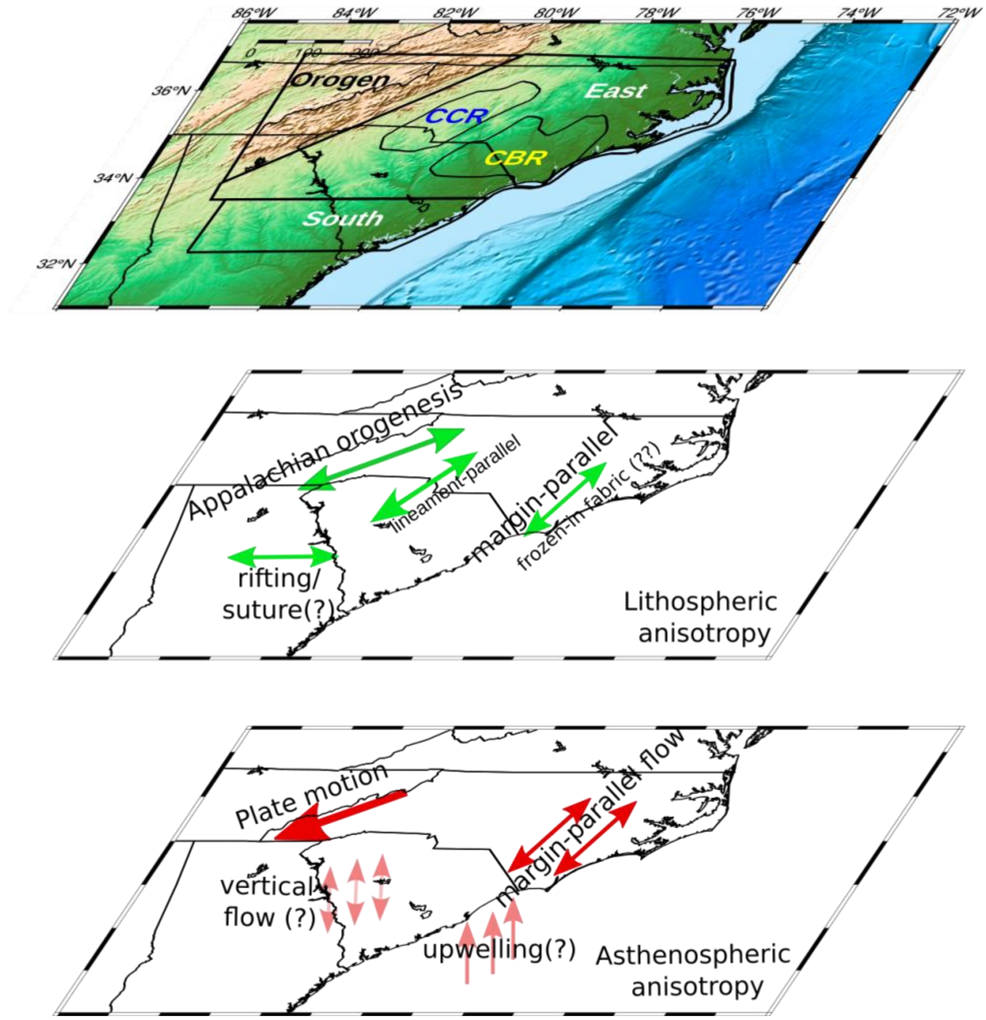

Figure 5.4 Preferred model of anisotropic structure beneath the southeastern US. There is a significant lithospheric contribution to splitting observed at the Appalachians even though asthenospheric component is possible as well. There may be lithospheric anisotropy related to the past collisional events and/or rifting which locally strengthen the splitting signal (e.g., at CBR and CCR). Along the coast, anisotropy is mostly due to asthenospheric source associated with edge-driven convection. Where nulls are dominant in the low frequency, a vertical component of flow might be present.

West of the CML, backazimuthal variations at station KMSC suggests both lithospheric and asthenospheric contributions to shear wave splitting. As KMSC is located near the Appalachians and therefore overlies the edge of the thicker orogenic lithosphere, significant lithospheric anisotropy is possible. In the asthenosphere, we expect modifications in the mantle flow system either due to horizontal deflection around the continental keel (Fouch et al., 2000) or small-scale edge-driven convection (King & Anderson, 1998). As it is located near the edge, more complex mantle flow could be prevalent beneath KMSC and would explain why there is a large scatter in the null backazimuths in the low and the splitting fast directions in the higher frequencies. There is either a strong lithospheric fabric or similar anisotropic contributions from both lithosphere and asthenosphere at the CCR that is recorded as splits in all three frequencies.

Overall, a principal lithospheric source of anisotropy related to the Appalachian orogenesis is present beneath the Appalachian Mountains. Asthenospheric anisotropy is likely present even if not significant. East of the Appalachians, most of the coast has vertical flow in the mantle except near eastern North Carolina-South Carolina where splitting is controlled by asthenospheric anisotropy that is dynamically driven. Collision as well as rift-related deformation are present in localized regions throughout the coastal plain. Together with asthenospheric anisotropy, these lithospheric sources result in the complex splitting patterns that we observe.

5.5 Limitations

Even though the change in splitting behavior with frequency tells us that the anisotropic properties are changing with depth, the path-integrated property of split measurements does not enable us to put unique depth constraints on the anisotropic structures (Long & Silver, 2009). This means that our interpreted layers could be either lithospheric or asthenospheric. Our attempt to model the layered anisotropy beneath KMSC revealed that two layers fit better than a single layer. However, the best-fit model is unable to explain all of the variation in the data observed. There could be further small-scale heterogeneities that we are not considering in the modeling. Most of our observations are made on arrivals from the western half of the circum-Pacific seismic belt. Because of the lack of measurements in the south-east quadrant, we cannot rule out the possibility that a more complex scenario of anisotropy could be present beneath KMSC.

Our high frequency data (1-5 s) is noisier than in the low and the mid frequencies. It is affected by the short-period noise generated due to ocean waves. The difference in site conditions between the orogen stations which are closer to bedrock compared to the coastal stations which have thicker sediment cover seems to be affecting the high frequency dataset. The lack of any measurements at the coastal stations in the high frequency is therefore a data quality issue. The general decrease in the number of measurements near the coast points out the limitations to using the high frequency range to detect splitting at noisier areas and areas with thick sediment cover where the high frequency energy gets more attenuated.

CONCLUSIONS

Our measurements of frequency-dependent shear wave splitting in seismic stations located in the eastern margin of the US reveal the presence of depth-dependent anisotropy with variable contributions from the lithosphere and the asthenosphere. In the Appalachian Mountains, although we argue for a significant lithospheric anisotropy, similar anisotropic geometry in both the lithosphere and the asthenosphere may have led to consistent splitting fast directions across all three frequencies used in the study. Just to the east of the Appalachians, there is evidence for multiple layers of anisotropy. Nulls in the low frequency and splits in the higher frequencies imply the presence of vertical flow in the asthenosphere and horizontal anisotropy in a relatively thin layer either in the lithosphere or in the asthenosphere. Along the coast, the coherent margin-parallel anisotropy is primarily in the asthenosphere. This margin-parallel anisotropy is likely related to the three-dimensional flow component of edge-driven convection. This explains why splitting is stronger at the North Carolina-South Carolina border closer to the low-velocity anomalies imaged in tomography studies and weaker further north and south. In the south, the nearly E-W fast directions could be either due to the collisional fabric imparted in the lithosphere during the Appalachian orogenesis or due to the Mesozoic rifting of Pangaea.

Our frequency-dependent results strongly support the presence of at least one strong anisotropic layer over the entire southeastern US with a strong possibility of vertical flow in the asthenospheric mantle beneath most of the Atlantic coastal plain. This explains why Long et al. (2016) observed mostly nulls in contrast to the N-S aligned splits measured by Yang et al. (2017) over the coastal plain. The depth and therefore the provenance of the anisotropic layers cannot be accurately determined from our analyses. However, there is abundant evidence that in the western part of the study region, frozen-in deformational fabrics are the main contributors to splitting, whereas along the coast, dynamics in the mantle are controlling the anisotropic fabric. Further constraints from techniques like anisotropy-aware receiver functions could help locate where the anisotropic properties change at depth. Our observations using multiple frequency bands will be an important complement to these studies in illuminating the anisotropic structure and provenance beneath the eastern margin.

REFERENCES

Abgarmi, B., & Arda Özacar, A. (2017). M-Split: A Graphical User Interface to Analyze Multilayered Anisotropy from Shear-Wave Splitting. *Seismological Research Letters*, *88*(4), 1146–1155. https://doi.org/10.1785/0220170020

Albuquerque Seismological Laboratory (ASL)/USGS. (1990). *United States National Seismic Network* [SEED data]. International Federation of Digital Seismograph Networks. https://doi.org/10.7914/SN/US

Alsina, D., & Snieder, R. (1995). Small-scale sublithospheric continental mantle deformation: Constraints from SKS splitting observations. *Geophysical Journal International*, *123*(2), 431–448. https://doi.org/10.1111/j.1365-246X.1995.tb06864.x

Aragon, J. C., Long, M. D., & Benoit, M. H. (2017). Lateral Variations in SKS Splitting Across the MAGIC Array, Central Appalachians. *Geochemistry, Geophysics, Geosystems*, *18*(11), 4136–4155. https://doi.org/10.1002/2017GC007169

Argus, D. F., Gordon, R. G., & DeMets, C. (2011). Geologically current motion of 56 plates relative to the no-net-rotation reference frame. *Geochemistry, Geophysics, Geosystems*, *12*(11). https://doi.org/10.1029/2011GC003751

Barruol, G., Helffrich, G., & Vauchez, A. (1997a). Shear wave splitting around the northern Atlantic: Frozen Pangaean lithospheric anisotropy? *Tectonophysics*, *279*(1–4), 135–148. https://doi.org/10.1016/S0040-1951(97)00126-1

Barruol, G., Silver, P. G., & Vauchez, A. (1997b). Seismic anisotropy in the eastern United States: Deep structure of a complex continental plate. *Journal of Geophysical Research: Solid Earth*, *102*(B4), 8329–8348. https://doi.org/10.1029/96JB03800

Benson, R. N. (2003). Age Estimates of the Seaward-Dipping Volcanic Wedge, Earliest Oceanic Crust, and Earliest Drift-Stage Sediments Along the North American Atlantic Continental Margin. In *The Central Atlantic Magmatic Province: Insights from Fragments of Pangea* (pp. 61–75). American Geophysical Union (AGU). https://doi.org/10.1029/136GM04

Biryol, C. B., Wagner, L. S., Fischer, K. M., & Hawman, R. B. (2016). Relationship between observed upper mantle structures and recent tectonic activity across the Southeastern United States. *Journal of Geophysical Research: Solid Earth*, *121*(5), 3393–3414. https://doi.org/10.1002/2015JB012698

Boote, S. K., Knapp, J. H., & Mueller, P. A. (2018). Preserved Neoproterozoic Continental Collision in Southeastern North America: The Brunswick Suture Zone and Osceola Continental Margin Arc. *Tectonics*, *37*(1), 305–321. https://doi.org/10.1002/2017TC004732

Bowman, J. R., & Ando, M. (1987). Shear-wave splitting in the upper-mantle wedge above the Tonga subduction zone. *Geophysical Journal International*, *88*(1), 25–41. https://doi.org/10.1111/j.1365-246X.1987.tb01367.x

Bromirski, P. D., Duennebier, F. K., & Stephen, R. A. (2005). Mid-ocean microseisms. *Geochemistry, Geophysics, Geosystems*, *6*(4). https://doi.org/10.1029/2004GC000768

Brunsvik, B. R., Eilon, Z. C., & Lynner, C. (2021). Mantle Structure and Flow Across the Continent-Ocean Transition of the Eastern North American Margin: Anisotropic *S* -Wave Tomography. *Geochemistry, Geophysics, Geosystems*, *22*(12). https://doi.org/10.1029/2021GC010084

Carrero Mustelier, E., & Menke, W. (2021). Seismic anomalies in the southeastern North American asthenosphere as characterized with body wave travel times from high-quality teleseisms. *Tectonophysics*, *809*, 228853. https://doi.org/10.1016/j.tecto.2021.228853

Chen, X., Li, Y., & Levin, V. (2018). Shear Wave Splitting Beneath Eastern North American Continent: Evidence for a Multilayered and Laterally Variable Anisotropic Structure. *Geochemistry, Geophysics, Geosystems*, *19*(8), 2857–2871. https://doi.org/10.1029/2018GC007646

Cherie, S. G., Gao, S. S., Liu, K. H., Elsheikh, A. A., Kong, F., Reed, C. A., & Yang, B. B. (2016). Shear wave splitting analyses in Tian Shan: Geodynamic implications of complex seismic anisotropy. *Geochemistry, Geophysics, Geosystems*, *17*(6), 1975–1989. https://doi.org/10.1002/2016GC006269

Crampin, S. (1994). The fracture criticality of crustal rocks. *Geophysical Journal International*, *118*(2), 428–438. https://doi.org/10.1111/j.1365-246X.1994.tb03974.x

Crampin, S., & Chastin, S. (2003). A review of shear wave splitting in the crack-critical crust. *Geophysical Journal International*, *155*(1), 221–240. https://doi.org/10.1046/j.1365-246X.2003.02037.x

Crampin, S., & Lovell, J. H. (1991). A decade of shear-wave splitting in the Earth's crust: What does it mean? what use can we make of it? and what should we do next? *Geophysical Journal International*, *107*(3), 387–407. https://doi.org/10.1111/j.1365-246X.1991.tb01401.x

Davis, J. K., Bécel, A., & Buck, W. R. (2018). Estimating emplacement rates for seaward-dipping reflectors associated with the U.S. East Coast Magnetic Anomaly. *Geophysical Journal International*, *215*(3), 1594–1603. https://doi.org/10.1093/gji/ggy360

Deschamps, F., Lebedev, S., Meier, T., & Trampert, J. (2008). Stratified seismic anisotropy reveals past and present deformation beneath the East-central United States. *Earth and Planetary Science Letters*, *274*(3–4), 489–498. https://doi.org/10.1016/j.epsl.2008.07.058

Dubé, J.-M., Darbyshire, F. A., Liddell, M. V., Stephenson, R., & Oakey, G. (2020). Seismic anisotropy of the Canadian High Arctic: Evidence from shear-wave splitting. *Tectonophysics*, *789*, 228524. https://doi.org/10.1016/j.tecto.2020.228524

Duff, P. D., & Kellogg, J. N. (2019). The Brunswick magnetic anomaly: Geophysical signature and geologic source. *Geology*, *47*(4), 355–358. https://doi.org/10.1130/G45462.1

Dziewonski, A. M., & Anderson, D. L. (1981). Preliminary reference Earth model. *Physics of the Earth and Planetary Interiors*, *25*(4), 297–356. https://doi.org/10.1016/0031-9201(81)90046-7

Eakin, C. M., & Long, M. D. (2013). Complex anisotropy beneath the Peruvian flat slab from frequency-dependent, multiple-phase shear wave splitting analysis. *Journal of Geophysical Research: Solid Earth*, *118*(9), 4794–4813. https://doi.org/10.1002/jgrb.50349

Eilon, Z., Abers, G. A., Jin, G., & Gaherty, J. B. (2014). Anisotropy beneath a highly extended continental rift. *Geochemistry, Geophysics, Geosystems*, *15*(3), 545–564. https://doi.org/10.1002/2013GC005092

Evans, Rob. L., Benoit, M. H., Long, M. D., Elsenbeck, J., Ford, H. A., Zhu, J., & Garcia, X. (2019). Thin lithosphere beneath the central Appalachian Mountains: A combined seismic and magnetotelluric study. *Earth and Planetary Science Letters*, *519*, 308–316. https://doi.org/10.1016/j.epsl.2019.04.046

Favier, N., & Chevrot, S. (2003). Sensitivity kernels for shear wave splitting in transverse isotropic media. *Geophysical Journal International*, *153*(1), 213–228. https://doi.org/10.1046/j.1365-246X.2003.01894.x

Fontaine, F. R., Barruol, G., Tommasi, A., & Bokelmann, G. H. R. (2007). Upper-mantle flow beneath French Polynesia from shear wave splitting. *Geophysical Journal International*, *170*(3), 1262–1288. https://doi.org/10.1111/j.1365-246X.2007.03475.x

Fouch, M. J., Fischer, K. M., Parmentier, E. M., Wysession, M. E., & Clarke, T. J. (2000). Shear wave splitting, continental keels, and patterns of mantle flow. *Journal of Geophysical Research: Solid Earth*, *105*(B3), 6255–6275. https://doi.org/10.1029/1999JB900372

Fouch, M. J., & Rondenay, S. (2006). Seismic anisotropy beneath stable continental interiors. *Physics of the Earth and Planetary Interiors*, *158*(2–4), 292–320. https://doi.org/10.1016/j.pepi.2006.03.024

Gaherty, J. B. (2004). A surface wave analysis of seismic anisotropy beneath eastern North America: Anisotropy beneath eastern North America. *Geophysical Journal International*, *158*(3), 1053–1066. https://doi.org/10.1111/j.1365-246X.2004.02371.x

Gao, H., & Li, C. (2021). Lithospheric Formation and Evolution of Eastern North American Continent. *Geophysical Research Letters*, *48*(5), e2020GL091074. https://doi.org/10.1029/2020GL091074

Gao, S. S., & Liu, K. H. (2009). Significant seismic anisotropy beneath the southern Lhasa Terrane, Tibetan Plateau. *Geochemistry, Geophysics, Geosystems*, *10*(2). https://doi.org/10.1029/2008GC002227

Gao, S. S., Liu, K. H., Stern, R. J., Keller, G. R., Hogan, J. P., Pulliam, J., & Anthony, E. Y. (2008). Characteristics of mantle fabrics beneath the south-central United States: Constraints from shear-wave splitting measurements. *Geosphere*, *4*(2), 411. https://doi.org/10.1130/GES00159.1

Gripp, A. E., & Gordon, R. G. (2002). Young tracks of hotspots and current plate velocities. *Geophysical Journal International*, *150*(2), 321–361. https://doi.org/10.1046/j.1365-246X.2002.01627.x

Grund, M., & Ritter, J. R. R. (2020). Shear-wave splitting beneath Fennoscandia—Evidence for dipping structures and laterally varying multilayer anisotropy. *Geophysical Journal International*, *223*(3), 1525–1547. https://doi.org/10.1093/gji/ggaa388

Guo, W., Zhao, S., Wang, F., Yang, Z., Jia, S., & Liu, Z. (2019). Crustal structure of the eastern Piedmont and Atlantic coastal plain in North Carolina and Virginia, eastern North American margin. *Earth, Planets and Space*, *71*(1), 69. https://doi.org/10.1186/s40623-019-1049-z

Guo, Z., & Chapman, M. C. (2019). An Examination of Amplification and Attenuation Effects in the Atlantic and Gulf Coastal Plain Using Spectral Ratios. *Bulletin of the Seismological Society of America*, *109*(5), 1855–1877. https://doi.org/10.1785/0120190071

Hatcher, R. D. (2007). Tectonic map of the southern and central Appalachians: A tale of three orogens and a complete Wilson cycle. In R. D. Hatcher (Ed.), *4-D Framework of Continental Crust*. Geological Society of America. https://doi.org/10.1130/2007.1200(29)

Hatcher, R. D. (2010). The Appalachian orogen: A brief summary. In R. P. Tollo, M. J. Bartholomew, J. P. Hibbard, & P. M. Karabinos, *From Rodinia to Pangea: The Lithotectonic Record of the Appalachian Region*. Geological Society of America. https://doi.org/10.1130/2010.1206(01)

Hibbard, J. P., Staal, C. R. V., & Rankin, D. W. (2007). A comparative analysis of pre-Silurian crustal building blocks of the northern and the southern Appalachian orogen. *American Journal of Science*, *307*(1), 23–45. https://doi.org/10.2475/01.2007.02

Higgins, M. W., & Zietz, I. (1983). Geologic interpretation of geophysical maps of the pre-Cretaceous “basement” beneath the Coastal Plain of the Southeastern United States. In R. D. Hatcher Jr., H. Williams, & I. Zietz (Eds.), *Contributions to the Tectonics and Geophysics of Mountain Chains* (Vol. 158, p. 0). Geological Society of America. https://doi.org/10.1130/MEM158-p125

Huang, Z., Tilmann, F., Xu, M., Wang, L., Ding, Z., Mi, N., Yu, D., & Li, H. (2017). Insight into NE Tibetan Plateau expansion from crustal and upper mantle anisotropy revealed by shear-wave splitting. *Earth and Planetary Science Letters*, *478*, 66–75. https://doi.org/10.1016/j.epsl.2017.08.030

Huang, Z., Zhao, D., & Wang, L. (2011). Frequency-dependent shear-wave splitting and multilayer anisotropy in northeast Japan. *Geophysical Research Letters*, *38*(8). https://doi.org/10.1029/2011GL046804

IRIS Transportable Array. (2003). *USArray Transportable Array* [SEED data]. International Federation of Digital Seismograph Networks. https://doi.org/10.7914/SN/TA

Jung, H., & Karato, S. (2001). Water-Induced Fabric Transitions in Olivine. *Science*, *293*(5534), 1460–1463. https://doi.org/10.1126/science.1062235

Kaislaniemi, L., & van Hunen, J. (2014). Dynamics of lithospheric thinning and mantle melting by edge-driven convection: Application to Moroccan Atlas mountains. *Geochemistry, Geophysics, Geosystems*, *15*(8), 3175–3189. https://doi.org/10.1002/2014GC005414

Karato, S., Jung, H., Katayama, I., & Skemer, P. (2008). Geodynamic Significance of Seismic Anisotropy of the Upper Mantle: New Insights from Laboratory Studies. *Annual Review of Earth and Planetary Sciences*, *36*(1), 59–95. https://doi.org/10.1146/annurev.earth.36.031207.124120

Katayama, I., Jung, H., & Karato, S. (2004). New type of olivine fabric from deformation experiments at modest water content and low stress. *Geology*, *32*(12), 1045. https://doi.org/10.1130/G20805.1

Kendall, J.-M., Pilidou, S., Keir, D., Bastow, I., Stuart, G., & Ayele, A. (2006). Mantle Upwellings, Melt Migration and the Rifting of Africa: Insights from Seismic Anisotropy. *Geological Society London Special Publications*, *259*, 55–72. https://doi.org/10.1144/GSL.SP.2006.259.01.06

Kendall, J.-M., Stuart, G. W., Ebinger, C. J., Bastow, I. D., & Keir, D. (2005). Magma-assisted rifting in Ethiopia. *Nature*, *433*(7022), Article 7022. https://doi.org/10.1038/nature03161

King, S. D. (2007). Hotspots and edge-driven convection. *Geology*, *35*(3), 223. https://doi.org/10.1130/G23291A.1

King, S. D., & Anderson, D. L. (1998). Edge-driven convection. *Earth and Planetary Science Letters*, *160*(3), 289–296. https://doi.org/10.1016/S0012-821X(98)00089-2

King, S. D., & Ritsema, J. (2000). African Hot Spot Volcanism: Small-Scale Convection in the Upper Mantle beneath Cratons. *Science*, *290*(5494), 1137–1140.

Kneller, E. A., van Keken, P. E., Karato, S., & Park, J. (2005). B-type olivine fabric in the mantle wedge: Insights from high-resolution non-Newtonian subduction zone models. *Earth and Planetary Science Letters*, *237*(3–4), 781–797. https://doi.org/10.1016/j.epsl.2005.06.049

Kong, F., Wu, J., Liu, L., Liu, K. H., Song, J., Li, J., & Gao, S. S. (2018). Azimuthal anisotropy and mantle flow underneath the southeastern Tibetan Plateau and northern Indochina Peninsula revealed by shear wave splitting analyses. *Tectonophysics*, *747–748*, 68–78. https://doi.org/10.1016/j.tecto.2018.09.013

Levin, V., Menke, W., & Park, J. (1999). Shear wave splitting in the Appalachians and the Urals: A case for multilayered anisotropy. *Journal of Geophysical Research: Solid Earth*, *104*(B8), 17975–17993. https://doi.org/10.1029/1999JB900168

Li, C., & Gao, H. (2021). Modification of Crust and Mantle Lithosphere Beneath the Southern Part of the Eastern North American Passive Margin. *Geophysical Research Letters*, *48*(16). https://doi.org/10.1029/2020GL090555

Li, Y., Wu, Q., Zhang, F., Feng, Q., & Zhang, R. (2011). Seismic anisotropy of the Northeastern Tibetan Plateau from shear wave splitting analysis. *Earth and Planetary Science Letters*, *304*(1), 147–157. https://doi.org/10.1016/j.epsl.2011.01.026

Liang, X., Zhao, D., Hua, Y., & Xu, Y.-G. (2022). Seismic Anisotropy Tomography and Mantle Dynamics of Central-Eastern USA. *Journal of Geophysical Research: Solid Earth*, *127*(12), e2022JB025484. https://doi.org/10.1029/2022JB025484

Liddell, M. V., Bastow, I., Darbyshire, F., Gilligan, A., & Pugh, S. (2017). The formation of Laurentia: Evidence from shear wave splitting. *Earth and Planetary Science Letters*, *479*, 170–178. https://doi.org/10.1016/j.epsl.2017.09.030

Long, M. D. (2010). Frequency-dependent shear wave splitting and heterogeneous anisotropic structure beneath the Gulf of California region. *Physics of the Earth and Planetary Interiors*, *182*(1–2), 59–72. https://doi.org/10.1016/j.pepi.2010.06.005

Long, M. D., & Becker, T. W. (2010). Mantle dynamics and seismic anisotropy. *Earth and Planetary Science Letters*, *297*(3–4), 341–354. https://doi.org/10.1016/j.epsl.2010.06.036

Long, M. D., Benoit, M. H., Chapman, M. C., & King, S. D. (2010). Upper mantle anisotropy and transition zone thickness beneath southeastern North America and implications for mantle dynamics. *Geochemistry, Geophysics, Geosystems*, *11*(10). https://doi.org/10.1029/2010GC003247

Long, M. D., Jackson, K. G., & McNamara, J. F. (2016). SKS splitting beneath Transportable Array stations in eastern North America and the signature of past lithospheric deformation. *Geochemistry, Geophysics, Geosystems*, *17*(1), 2–15. https://doi.org/10.1002/2015GC006088

Long, M. D., & Silver, P. G. (2009). Shear Wave Splitting and Mantle Anisotropy: Measurements, Interpretations, and New Directions. *Surveys in Geophysics*, *30*(4–5), 407–461. https://doi.org/10.1007/s10712-009-9075-1

Long, M. D., Wagner, L. S., King, S. D., Evans, R. L., Mazza, S. E., Byrnes, J. S., Johnson, E. A., Kirby, E., Bezada, M. J., Gazel, E., Miller, S. R., Aragon, J. C., & Liu, S. (2021). Evaluating Models for Lithospheric Loss and Intraplate Volcanism Beneath the Central Appalachian Mountains. *Journal of Geophysical Research: Solid Earth*, *126*(10), e2021JB022571. https://doi.org/10.1029/2021JB022571

Lynner, C., & Bodmer, M. (2017). Mantle flow along the eastern North American margin inferred from shear wave splitting. *Geology*, *45*(10), 867–870. https://doi.org/10.1130/G38980.1

Lynner, C., J. A. Van Avendonk, H., Bécel, A., Christeson, G. L., Dugan, B., Gaherty, J. B., Harder, S., Hornbach, M. J., Lizarralde, D., Long, M. D., Magnani, M. B., Shillington, D. J., Aderhold, K., Eilon, Z. C., & Wagner, L. S. (2019). The Eastern North American Margin Community Seismic Experiment: An Amphibious Active- and Passive-Source Dataset. *Seismological Research Letters*, *91*(1), 533–540. https://doi.org/10.1785/0220190142

Lynner, C., Long, M. D., Thissen, C. J., Paczkowski, K., & Montési, L. G. J. (2017). Evaluating geodynamic models for sub-slab anisotropy: Effects of olivine fabric type. *Geosphere*, *13*(2), 247–259. https://doi.org/10.1130/GES01395.1

Lynner, C., & Porritt, R. W. (2017). Crustal structure across the eastern North American margin from ambient noise tomography. *Geophysical Research Letters*, *44*(13), 6651–6657. https://doi.org/10.1002/2017GL073500

Mainprice, D., Barruol, G., & Ismaïl, W. B. (2000). The Seismic anisotropy of the Earth's mantle: From single crystal to polycrystal. In S. Karato, A. Forte, R. Liebermann, G. Masters, & L. Stixrude (Eds.), *Geophysical Monograph Series* (Vol. 117, pp. 237–264). American Geophysical Union. https://doi.org/10.1029/GM117p0237

Marson-Pidgeon, K., & Savage, M. K. (1997). Frequency-dependent anisotropy in Wellington, New Zealand. *Geophysical Research Letters*, *24*(24), 3297–3300. https://doi.org/10.1029/97GL03274

Marson-Pidgeon, K., & Savage, M. K. (2004). Modelling shear wave splitting observations from Wellington, New Zealand. *Geophysical Journal International*, *157*(2), 853–864. https://doi.org/10.1111/j.1365-246X.2004.02274.x

Marzen, R. E., Shillington, D. J., Lizarralde, D., & Harder, S. H. (2019). Constraints on Appalachian Orogenesis and Continental Rifting in the Southeastern United States From Wide-Angle Seismic Data. *Journal of Geophysical Research: Solid Earth*, *124*(7), 6625–6652. https://doi.org/10.1029/2019JB017611

Marzoli, A., Callegaro, S., Dal Corso, J., Davies, J. H. F. L., Chiaradia, M., Youbi, N., Bertrand, H., Reisberg, L., Merle, R., & Jourdan, F. (2018). The Central Atlantic Magmatic Province (CAMP): A Review. In L. H. Tanner (Ed.), *The Late Triassic World: Earth in a Time of Transition* (pp. 91–125). Springer International Publishing. https://doi.org/10.1007/978-3-319-68009-5_4

Mazza, S. E., Gazel, E., Johnson, E. A., Kunk, M. J., McAleer, R., Spotila, J. A., Bizimis, M., & Coleman, D. S. (2014). Volcanoes of the passive margin: The youngest magmatic event in eastern North America. *Geology*, *42*(6), 483–486. https://doi.org/10.1130/G35407.1

Mueller, P. A., Heatherington, A. L., Foster, D. A., Thomas, W. A., & Wooden, J. L. (2014). The Suwannee suture: Significance for Gondwana-Laurentia terrane transfer and formation of Pangaea. *Gondwana Research*, *26*(1), 365–373. https://doi.org/10.1016/j.gr.2013.06.018

Murphy, B. S., & Egbert, G. D. (2019). Synthesizing Seemingly Contradictory Seismic and Magnetotelluric Observations in the Southeastern United States to Image Physical Properties of the Lithosphere. *Geochemistry, Geophysics, Geosystems*, *20*(6), 2606–2625. https://doi.org/10.1029/2019GC008279

Nicolas, A. (1993). Why fast polarization directions of SKS seismic waves are parallel to mountain belts. *Physics of the Earth and Planetary Interiors*, *78*(3–4), 337–342. https://doi.org/10.1016/0031-9201(93)90164-5

Özalaybey, S., & Savage, M. K. (1994). Double-layer anisotropy resolved from *S* phases. *Geophysical Journal International*, *117*(3), 653–664. https://doi.org/10.1111/j.1365-246X.1994.tb02460.x

Parker, E. H., Jr. (2014). Crustal magnetism, tectonic inheritance, and continental rifting in the southeastern United States. *GSA Today*, *24*(4), 4–9. https://doi.org/10.1130/GSAT-G192A.1

Parker, E. H., Jr., Hawman, R. B., Fischer, K. M., & Wagner, L. S. (2013). Crustal evolution across the southern Appalachians: Initial results from the SESAME broadband array. *Geophysical Research Letters*, *40*(15), 3853–3857. https://doi.org/10.1002/grl.50761

Polet, J., & Kanamori, H. (2002). Anisotropy beneath California: Shear wave splitting measurements using a dense broadband array. *Geophysical Journal International*, *149*(2), 313–327. https://doi.org/10.1046/j.1365-246X.2002.01630.x

Pollitz, F. F., & Mooney, W. D. (2016). Seismic velocity structure of the crust and shallow mantle of the Central and Eastern United States by seismic surface wave imaging. *Geophysical Research Letters*, *43*(1), 118–126. https://doi.org/10.1002/2015GL066637

Porritt, R. W., Becker, T. W., Boschi, L., & Auer, L. (2021). Multiscale, radially anisotropic shear wave imaging of the mantle underneath the contiguous United States through joint inversion of USArray and global data sets. *Geophysical Journal International*, *226*(3), 1730–1746. https://doi.org/10.1093/gji/ggab185

Ragland, P. C., Hatcher, R. D., Jr., & Whittington, D. (1983). Juxtaposed Mesozoic diabase dike sets from the Carolinas: A preliminary assessment. *Geology*, *11*(7), 394–399. https://doi.org/10.1130/0091-7613(1983)11<394:JMDDSF>2.0.CO;2

Ritter, J. R. R., Fröhlich, Y., Sanz Alonso, Y., & Grund, M. (2022). Short-scale laterally varying SK(K)S shear wave splitting at BFO, Germany—Implications for the determination of anisotropic structures. *Journal of Seismology*, *26*(6), 1137–1156. https://doi.org/10.1007/s10950-022-10112-w

Rümpker, G., & Ryberg, T. (2000). New “Fresnel-Zone” estimates for shear-wave splitting observations from finite-difference modeling. *Geophysical Research Letters*, *27*(13), 2005–2008. https://doi.org/10.1029/2000GL011423

Rümpker, G., & Silver, P. G. (1998). Apparent shear-wave splitting parameters in the presence of vertically varying anisotropy. *Geophysical Journal International*, *135*(3), 790–800. https://doi.org/10.1046/j.1365-246X.1998.00660.x

Rümpker, G., Tommasi, A., & Kendall, J.-M. (1999). Numerical simulations of depth-dependent anisotropy and frequency-dependent wave propagation effects. *Journal of Geophysical Research: Solid Earth*, *104*(B10), 23141–23153. https://doi.org/10.1029/1999JB900203

Russell, J. B., & Gaherty, J. B. (2021). Lithosphere Structure and Seismic Anisotropy Offshore Eastern North America: Implications for Continental Breakup and Ultra-Slow Spreading Dynamics. *Journal of Geophysical Research: Solid Earth*, *126*(12). https://doi.org/10.1029/2021JB022955

Saltzer, R. L., Gaherty, J. B., & Jordan, T. H. (2000). How are vertical shear wave splitting measurements affected by variations in the orientation of azimuthal anisotropy with depth? *Geophysical Journal International*, *141*(2), 374–390. https://doi.org/10.1046/j.1365-246x.2000.00088.x

Savage, B. (2021). Body Wave Speed Structure of Eastern North America. *Geochemistry, Geophysics, Geosystems*, *22*(1). https://doi.org/10.1029/2020GC009002

Savage, B., Covellone, B. M., & Shen, Y. (2017). Wave speed structure of the eastern North American margin. *Earth and Planetary Science Letters*, *459*, 394–405. https://doi.org/10.1016/j.epsl.2016.11.028

Savage, M. K. (1999). Seismic anisotropy and mantle deformation: What have we learned from shear wave splitting? *Reviews of Geophysics*, *37*(1), 65–106. https://doi.org/10.1029/98RG02075

Savage, Martha Kane, & Silver, P. G. (1993). Mantle deformation and tectonics: Constraints from seismic anisotropy in the western United States. *Physics of the Earth and Planetary Interiors*, *78*(3), 207–227. https://doi.org/10.1016/0031-9201(93)90156-4

Schlische, R. W. (2003). Progress in Understanding the Structural Geology, Basin Evolution, and Tectonic History of the Eastern North American Rift System. In P. M. LeTourneau & P. E. Olsen (Eds.), *The Great Rift Valleys of Pangea in Eastern North America* (Vol. 1, pp. 21–64). Columbia University Press. https://doi.org/10.7312/leto11162-003

Schmandt, B., & Lin, F.-C. (2014). *P* and *S* wave tomography of the mantle beneath the United States. *Geophysical Research Letters*, *41*(18), 6342–6349. https://doi.org/10.1002/2014GL061231

Schmid, C., van der Lee, S., & Giardini, D. (2004). Delay times and shear wave splitting in the Mediterranean region. *Geophysical Journal International*, *159*(1), 275–290. https://doi.org/10.1111/j.1365-246X.2004.02381.x

Silver, P. G. (1996). Seismic Anisotropy Beneath the Continents: Probing the Depths of Geology. *Annual Review of Earth and Planetary Sciences*, *24*(1), 385–432. https://doi.org/10.1146/annurev.earth.24.1.385

Silver, P. G., & Chan, W. W. (1988). Implications for continental structure and evolution from seismic anisotropy. *Nature*, *335*(6185), 34–39. Scopus. https://doi.org/10.1038/335034a0

Silver, P. G., & Chan, W. W. (1991). Shear wave splitting and subcontinental mantle deformation. *Journal of Geophysical Research: Solid Earth*, *96*(B10), 16429–16454. https://doi.org/10.1029/91JB00899

Silver, P. G., & Savage, M. K. (1994). The Interpretation of Shear-Wave Splitting Parameters In the Presence of Two Anisotropic Layers. *Geophysical Journal International*, *119*(3), 949–963. https://doi.org/10.1111/j.1365-246X.1994.tb04027.x

Taylor, P., Zietz, I., & Dennis, L. S. (1968). Geologic implications of aeromagnetic data for the eastern continental margin of the United States. *Geophysics*, *33*(5), 755–780. https://doi.org/10.1190/1.1439970

Thomas, W. A. (2006). Tectonic inheritance at a continental margin. *GSA Today*, *16*(2), 4. https://doi.org/10.1130/1052-5173(2006)016[4:TIAACM]2.0.CO;2

Tommasi, A., Tikoff, B., & Vauchez, A. (1999). Upper mantle tectonics: Three-dimensional deformation, olivine crystallographic fabrics and seismic properties. *Earth and Planetary Science Letters*, *168*(1), 173–186. https://doi.org/10.1016/S0012-821X(99)00046-1

van der Lee, S. (2002). High-resolution estimates of lithospheric thickness from Missouri to Massachusetts, USA. *Earth and Planetary Science Letters*, *203*(1), 15–23. https://doi.org/10.1016/S0012-821X(02)00846-4

van der Lee, S., & Nolet, G. (1997). Upper mantle S velocity structure of North America. *Journal of Geophysical Research: Solid Earth*, *102*(B10), 22815–22838. https://doi.org/10.1029/97JB01168 van der Lee, S., Regenauer-Lieb, K., & Yuen, D. A. (2008). The role of water in connecting past and future episodes of subduction. *Earth and Planetary Science Letters*, *273*(1), 15–27. https://doi.org/10.1016/j.epsl.2008.04.041

Vauchez, A., & Barruol, G. (1996). Shear-wave splitting in the Appalachians and the Pyrenees: Importance of the inherited tectonic fabric of the lithosphere. *Physics of the Earth and Planetary Interiors*, *95*(3), 127–138. https://doi.org/10.1016/0031-9201(95)03125-1

Vauchez, A., & Nicolas, A. (1991). Mountain building: Strike-parallel motion and mantle anisotropy. *Tectonophysics*, *185*(3), 183–201. https://doi.org/10.1016/0040-1951(91)90443-V

Vauchez, A., Tommasi, A., Barruol, G., & Maumus, J. (2000). Upper mantle deformation and seismic anisotropy in continental rifts. *Physics and Chemistry of the Earth, Part A: Solid Earth and Geodesy*, *25*(2), 111–117. https://doi.org/10.1016/S1464-1895(00)00019-3

Wagner, L. S., Fischer, K. M., Hawman, R., Hopper, E., & Howell, D. (2018). The relative roles of inheritance and long-term passive margin lithospheric evolution on the modern structure and tectonic activity in the southeastern United States. *Geosphere*, *14*(4), 1385–1410. https://doi.org/10.1130/GES01593.1

Wagner, L. S., Long, M. D., Johnston, M. D., & Benoit, M. H. (2012). Lithospheric and asthenospheric contributions to shear-wave splitting observations in the southeastern United States. *Earth and Planetary Science Letters*, *341–344*, 128–138. https://doi.org/10.1016/j.epsl.2012.06.020

Walker, K. T., Bokelmann, G. H. R., Klemperer, S. L., & Bock, G. (2005). Shear-wave splitting around the Eifel hotspot: Evidence for a mantle upwelling. *Geophysical Journal International*, *163*(3), 962–980. https://doi.org/10.1111/j.1365-246X.2005.02636.x

White-Gaynor, A. L., & Nyblade, A. A. (2017a). Shear wave splitting across the Mid-Atlantic region of North America: A fossil anisotropy interpretation. *Geology*, *45*(6), 555–558. https://doi.org/10.1130/G38794.1

White-Gaynor, A. L., & Nyblade, A. A. (2017b). Shear wave splitting across the Mid-Atlantic region of North America: A fossil anisotropy interpretation. *Geology*, *45*(6), 555–558. https://doi.org/10.1130/G38794.1

Wirth, E., & Long, M. D. (2010). Frequency-dependent shear wave splitting beneath the Japan and Izu-Bonin subduction zones. *Physics of the Earth and Planetary Interiors*, *181*(3), 141–154. https://doi.org/10.1016/j.pepi.2010.05.006

Withjack, M. O., Schlische, R., & Olsen, P. (2012). *Development of the passive margin of Eastern North America* (pp. 300–335). https://doi.org/10.1016/B978-0-444-56356-9.00012-2

Withjack, M. O., & Schlische, R. W. (2005). A Review of Tectonic Events on the Passive Margin of Eastern North America. In P. J. Post, N. C. Rosen, D. L. Olson, S. L. Palmes, K. T. Lyons, & G. B. Newton (Eds.), *Petroleum Systems of Divergent Continental Margin Basins* (Vol. 25, p. 0). SEPM Society for Sedimentary Geology. https://doi.org/10.5724/gcs.05.25.0203

Wüstefeld, A., & Bokelmann, G. (2007). Null Detection in Shear-Wave Splitting Measurements. *Bulletin of the Seismological Society of America*, *97*(4), 1204–1211. https://doi.org/10.1785/0120060190

Wüstefeld, A., Bokelmann, G., & Barruol, G. (2010). Evidence for ancient lithospheric deformation in the East European Craton based on mantle seismic anisotropy and crustal magnetics. *Tectonophysics*, *481*(1–4), 16. https://doi.org/10.1016/j.tecto.2009.01.010

Wüstefeld, A., Bokelmann, G., Zaroli, C., & Barruol, G. (2008). SplitLab: A shear-wave splitting environment in Matlab. *Computers & Geosciences*, *34*(5), 515–528. https://doi.org/10.1016/j.cageo.2007.08.002

Yang, B. B., Liu, Y., Dahm, H., Liu, K. H., & Gao, S. S. (2017). Seismic azimuthal anisotropy beneath the eastern United States and its geodynamic implications: EASTERN U.S. SEISMIC ANISOTROPY. *Geophysical Research Letters*, *44*(6), 2670–2678. https://doi.org/10.1002/2016GL071227

Yuan, H., & Romanowicz, B. (2010). Lithospheric layering in the North American craton. *Nature*, *466*(7310), 1063–1068. https://doi.org/10.1038/nature09332

Yuan, H., Romanowicz, B., Fischer, K. M., & Abt, D. (2011). 3-D shear wave radially and azimuthally anisotropic velocity model of the North American upper mantle. *Geophysical Journal International*, *184*(3), 1237–1260. https://doi.org/10.1111/j.1365-246X.2010.04901.x